

X-ray Tomography and Tomoscopy on Metals: A Review

Francisco García-Moreno,* Tillmann Robert Neu, Paul Hans Kamm, and John Banhart

X-ray tomography is a versatile tool in materials research and engineering since it allows for a non-destructive and three-dimensional mapping of the constituents of a heterogeneous material as long as they differ in their interactions with X-rays. Recent developments of the technique have brought down the time needed for the acquisition of a single tomogram by many orders of magnitude compared to what was needed 25 years ago. Nowadays, up to 1000 full tomograms can be recorded in a second, which enables real-time studies of changes in samples caused by reactions or by applied processing operations. The term tomoscopy has been coined for such sequences of 3D images. We review the application of X-ray tomography and tomoscopy on metals and describe each step required and the associated challenges. A selection of representative investigations is presented with a focus on time-resolved phenomena in metals and alloys ranging from mechanical deformation, solidification to metals processing processes such as welding and additive manufacturing. Finally likely future developments are discussed.

most suitable for studying a given material depends on the interaction between the applied radiation and the material, the length scale of phenomena to be studied and, more generally, the specific scientific question to be answered. Whenever materials are changing in time and such changes have to be monitored, e.g., during chemical or metallurgical reactions or a manufacturing process, non-destructive methods are mandatory, which influence the evolution of the system only marginally. This review deals with metallic materials, which restricts the range of suitable techniques. In particular, we will focus on X-ray tomographic methods.

1.2. Imaging Methods

The macro- and microstructure of metallic materials such as grains, intermetallic phases, various types of defects, constituent arrangements, etc., can be studied by X-ray radiography or tomography. A standard analysis strategy for the characterisation of solid samples is to obtain a 2D image (radiograph or radiogram) or 3D volume image (tomogram) of the structure, which can be further analysed by various methods of image analysis.

Time-dependent properties such as changes induced by mechanical or thermal stresses as well as changes caused by materials processing or synthesis can be investigated by preparing samples under different conditions or in different stages of evolution and characterising the resulting series of samples by X-ray radiography or tomography post-mortem or ex-situ in a different environment. Such studies are limited by the scatter in properties caused by not exactly reproducible starting and processing conditions and by possible changes caused by the interruption of a reaction or during subsequent measurement (Figure 1a). In some cases, one can subject a single sample to multiple incremental processing steps and take images after each step. For example, one can load a sample to increasingly higher levels and observe yielding through a series of images taken ex-situ after unloading. What remains here is the difficulty of positioning samples precisely enough to ensure that a series of images taken of the samples show the same features at the same location. Moreover, there is a practical limit of the number of incremental steps that can be applied (Figure 1b). A better option is not to remove the sample from the tomographic stage but stop the process and take a series of tomograms after each step, which is called quasi-in-situ or interrupted imaging (Figure 1c). A more efficient and elegant way, and very often the only way of process analysis, is the time-resolved and truly in-situ tomography (Figure 1d). Truly means that a reaction of


1. Introduction

1.1. General Introduction

The structure and properties of materials can be evaluated by a wide range of techniques, which can be divided into destructive and non-destructive methods. The latter may be based on acoustic, electric, magnetic, optical or radiographic principles and include many techniques summarised as non-destructive evaluation (NDE) or non-destructive testing (NDT).^[1] The most common radiation-based methods are spectroscopy, scattering, diffraction, and imaging. Radiation imaging utilises electromagnetic radiation all through the energy spectrum from microwaves to γ -rays, particle radiation such as protons, electrons, neutrons, or other waves such as sound waves. Which imaging method is

F. García-Moreno, T. R. Neu, P. H. Kamm, J. Banhart
Institute of Applied Materials
Helmholtz-Zentrum Berlin für Materialien und Energie
Hahn-Meitner-Platz 1, 14109 Berlin, Germany
E-mail: garcia-moreno@helmholtz-berlin.de

F. García-Moreno, T. R. Neu, P. H. Kamm, J. Banhart
Institute of Materials Science and Technology
Technische Universität Berlin
Hardenbergstr. 36, 10623 Berlin, Germany

 The ORCID identification number(s) for the author(s) of this article can be found under <https://doi.org/10.1002/adem.202201355>.

© 2022 The Authors. Advanced Engineering Materials published by Wiley-VCH GmbH. This is an open access article under the terms of the Creative Commons Attribution License, which permits use, distribution and reproduction in any medium, provided the original work is properly cited.

DOI: 10.1002/adem.202201355

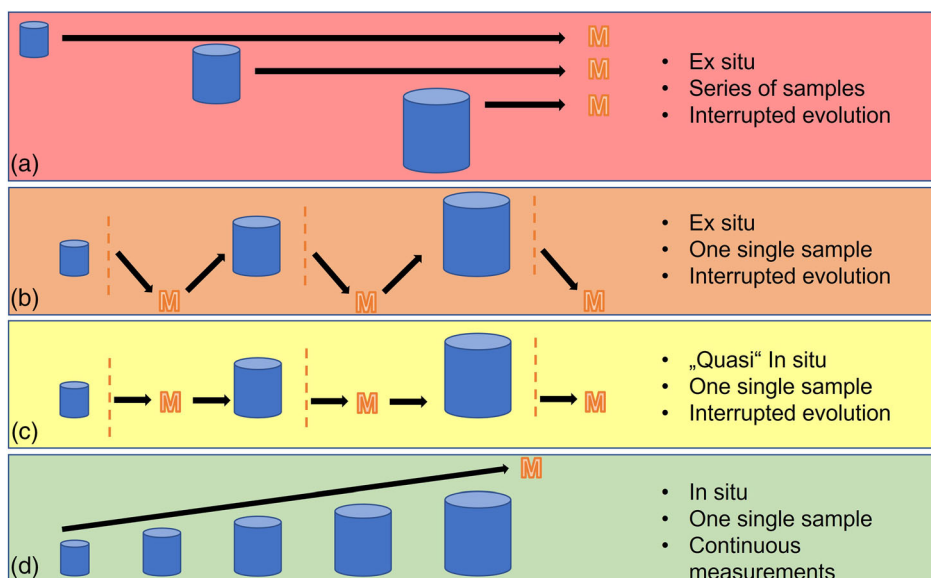


Figure 1. Schematic depiction of various strategies to obtain time-resolved tomographic data representing an evolving sample. *M* stands for measurement and vertical dashes for an interruption of a process evolving the sample (blue cylinder) from small to large. The size of the sample symbolises their different stadia of evolution.

process is not interrupted or slowed down for measurement. For example, in the course of temperature-dependent processing the sample is neither cooled to a measuring temperature nor removed from its location.

Continuous measurements (Figure 1d) are indeed possible up to very high rotation speeds (up to 500 Hz), so that the samples are not affected in a significant way by the radial *g*-forces. For *g*-forces beyond gravitational forces, this must be checked in each individual case study. The limits of sample rotation speed depend mainly on the type of sample and the processing parameters. For example, some solidifying AlBi10 samples could not be analysed at high rotational speeds because segregation of Bi droplets was observed at the sample edges. On the other hand, some liquid, but quite viscous metal foams, did not show significant variations in foam density, indicating that the influence is marginal.^[2,3]

Measurements techniques have become faster and more applicable in the recent years due to technological developments, thus opening new opportunities for studies of a large number of materials science questions including dynamic processes, which hitherto could not be studied. Recently the term *operando* investigation is increasingly being used for measurements where the operation of a device or a reaction chamber is monitored by measurements *in situ*. In this context, a well-thought-out design and a suitable sample environment play a predominant role, as the set-ups must reproduce the real process but at the same time fulfil the tomographic requirements, e.g., a rotating sample. One route that is often taken, although often difficult to realize, is a non-contact sample environment.^[2]

1.3. Types of Tomography

The word tomography is derived from the Greek word stems *tomos*, meaning slice or section, and *graphos*, meaning image. It

provides a visualization of the component distribution inside materials displayed through cross-sectional or three-dimensional images, which can be further processed and quantitatively evaluated.^[4,5]

The term tomography is used in a general sense for a variety of methods including both destructive and non-destructive ones. The former category includes sectional slicing techniques such as focussed ion beam tomography (FIB)^[6,7] or 3D atom probe tomography (3DAP), which is based on atomic ablation.^[8–10] Among the non-destructive methods are: neutron tomography,^[11] ultrasound tomography,^[12] electrical tomography,^[13] optical coherence tomography,^[14] electron tomography,^[15] positron emission tomography^[16] and X-ray tomography.^[4,17]

Since X-ray based imaging has become available medicine has taken the biggest advantage of it and triggered its further development.^[18–20] However, tomography is nowadays widespread in other research fields such as materials science,^[21,22] biology,^[23] geoscience,^[24] archaeology^[25] or even fluid dynamics.^[26] Furthermore, tomography is gaining more and more acceptance in industry^[27] for non-destructive testing,^[28–30] reverse engineering,^[31] defect detection,^[1] material inspection^[32] or quality control.^[28,33]

1.4. Medical Computer Tomography

In 1972, the first medical X-ray tomography scanner was presented by Hounsfield,^[34] who obtained the Nobel Prize in medicine for the development of computer assisted tomography (CAT/CT) in 1979. Fast computer tomography (CT) was introduced into medicine about four decades ago and was mainly used for cardiovascular diagnostics. In 1982, a remarkable high-speed, multi-slice, X-ray CT technique with an acquisition of 8 slices in a total of 100–200 ms (one slice in 30–50 ms) and one tomogram per second in a continuous mode was

presented.^[35] This method was improved in 1985 by the denominated rapid acquisition computer axial tomography (RACAT), which allowed up to 17 tomograms per second to be acquired, with 4 slices (8 mm thick each) per tomogram separated by 12 mm and with an exposure time of 50 ms.^[36] RACAT was improved and “re-baptized” to ultrafast computed tomography or cinetomography in 1986, and was dedicated to the study of heart function and allowed for acquiring up to 11 slices per tomogram.^[37] Although these acquisition rates were very impressive at that time, time resolution was pushed up at the cost of spatial resolution, contrast and number of slices.

1.5. Gas-Liquid Flow Dynamics

Another research area that promoted the development of time-resolved tomography is gas-liquid flow dynamics. In 1991, tomographic analyses of fluidized and trickle beds were produced with 1 single slice and a pixel size of 0.5 mm × 0.5 mm at a speed of 0.038 slices per second.^[38] Some years later a temporal improvement to 0.33 slices per second and a pixel size of 0.4 mm × 0.4 mm was achieved by the commercial scanner EMI 7070, which allowed for a transversal motion of 1–10 mm.^[39] In parallel to this scanner, the development of the switching e-beam scanning concept for liquid flow visualization (no rotation of sample, target or detector needed) increased the acquisition velocity by several orders of magnitude up to 250 slices per second with 1.5 mm spatial resolution.^[40] In 2006, more than one decade later, ultrafast tomography with 1000 slices per second and a spatial resolution of ≈1 mm was presented.^[41,42] In 2016, this method was improved to 8000 slices per second with a voxel size of 0.5 mm^[26] by the Rossendorf fast electron beam X-ray tomography (ROFEX) instrument, which is the most recent configuration of the e-beam scanning concept and remains up to present.^[43]

1.6. X-ray Tomoscopy

The continuous development of synchrotron radiation sources and the latest advances in the performance of sensors, cameras and detectors have triggered a rapid improvement of in-situ techniques in the past years and this trend continues. One of these techniques is the time-resolved imaging of materials evolution and manufacturing processes. Often this option is the only way to go, for example when studying the solidification of metallic alloys or evolution of damage since intermediary stages are hard or even impossible to preserve. In the simplest case, this is radiography, where 2D radiograms of the X-ray absorption distribution in a material are obtained to reveal its internal structure. For constituents with similar X-ray absorption coefficients, phase contrast can be exploited to distinguish these constituents.^[44,45] It has become customary to call the acquisition of series of radiograms of a changing object radioscopy.^[46]

By acquiring a defined number of radiograms from different angles of view, also called projections, followed by numerical reconstruction of the three-dimensional structure, one advances to tomography.^[5] Tomography avoids the ambiguities and interpretations of radiography caused by the superposition of features along the direction of the rays and the associated loss of information, and allows for more quantitative analyses.^[4]

Whenever the temporal resolution allows for performing in-situ investigations, tomography evolves to tomoscopy. The suffix scopy means a study or examination, in this case of a process or evolution, containing more information than a simple image, graphy. The term tomoscopy was introduced in 1970 as an expression for time-resolved tomography for the fluoroscopic observation under different angles of rapidly repeated X-ray exposures,^[47] and further used 1982 for dynamic medical observations using a rotating anode X-ray tube.^[48] Although these methods produced impressive results at that time, spatial and temporal resolutions were much rougher than those available today.^[2] The focus of modern experiments is shifting to dynamic, in-situ or operando analyses rather than on simple traditional tomography of solid samples. Tomoscopy is also called time-resolved or 4D (3 spatial + a temporal component) tomography. The latter term is ambiguous since spectral or scattering properties are sometimes also counted as dimension, which even leads to terms like 5D tomography.^[49]

Laboratory X-ray scanners are nowadays very flexible, widespread, and powerful, and benefit from improved spatial and temporal resolutions. Some commercial ones are capable of acquisition velocities of 1 tomogram in 6 s under favourable conditions,^[50] and some experimental setups even below one second.^[51]

Nevertheless, cutting-edge experiments are still restricted to highly brilliant synchrotron X-ray sources. An overview of the evolution of temporal resolution of tomoscopy with spatial resolutions in the micrometer range or better since 1995 in terms of acquisition time expressed by number of tomograms per second (tps) as reported in the literature and extracted from the Tomoscopy Experiments database is shown in **Figure 2**.^[52] Here we can observe that the temporal resolution has improved by almost 5 orders of magnitude over the past 20 years.

High-intensity single-bunch synchrotron radiation allows for very short exposure times down to 100 ps for a single image at high spatial resolutions^[53] and X-ray free-electron lasers allow for

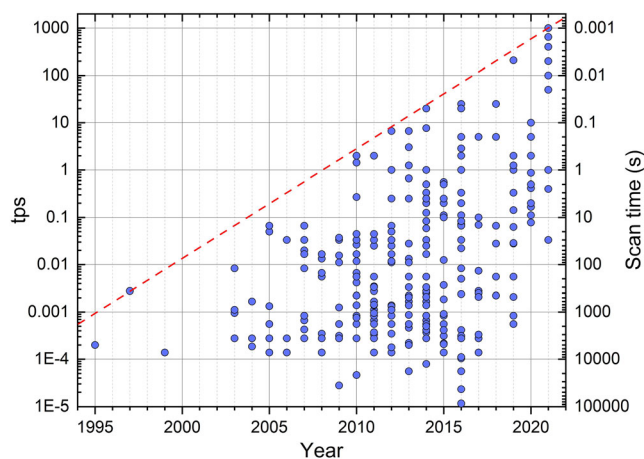


Figure 2. Development of the temporal resolution of tomoscopy with pixel size in the micrometer range since 1995 in terms of scan time or tomograms per second reported in the literature and extracted from the database.^[52] The broken red line denotes an approximate value for the highest available scan rate at all the available tomography setups over time.

an image acquisition in the femtosecond range,^[54,55] but with a very restricted total acquisition time.

1.7. In this Work

This manuscript reviews the main fields of metallic materials research studied in the past decade through X-ray tomography and tomoscopy. The application of the methods spans a range from fairly well-researched areas such as morphological characterisations including structural defects, grain structures, distributions of phases, porosities, etc. to the latest studies, especially concerning fast dynamic processes, which can be studied with tomoscopy at high rates. Such processes include phase transformations or separations, behaviour under mechanical stress and deformation, failure, semi-solid forming, solidification, gas nucleation, foam evolution, thermal combustion, sintering, laser processing, etc. The focus of this work lies on both established activities of the past years and developments of new time-resolving methods and associated challenges as well as on several recent and inspirational cutting-edge experiments and novel case studies that are described in more detail.

Besides X-ray attenuation or X-ray phase contrast based tomography, other kinds of three-dimensional imaging exist including 3D X-ray diffraction microscopy (3DXRD)^[56–58] or diffraction contrast tomography (DCT),^[56] which reveal the crystallographic orientation of domains in metals, or X-ray Absorption Near Edge Structure (XANES),^[59] which shows spatial variations in chemistry. Such methods are beyond the scope of this review.

2. Experimental Section

2.1. Basic Concepts

The first step in planning a tomographic experiment is to consider various aspects and parameters that determine the experimental output; field of view, spatial and temporal resolution, and other factors must be adjusted depending on the available X-ray flux and energy such as type of scintillator, optical system, camera performance, material absorption, sample size, etc. For example, spatial resolution and exposure time must be adapted to the sample volume and contrast desired. Due to the high X-ray absorption of many metals, conventional attenuation contrast is usually applied in a wide range of works, although, in special cases, a certain amount of phase contrast can be beneficial to distinguish between phases with similar density and absorption.

The X-ray flux available determines the rate of incident photons on a sample, which in addition to the efficiency and readout time of the detector system determines the exposure time required for a single projection and therefore eventually defines the temporal resolution that can be achieved, which is a key parameter for tomoscopy. Typically, spatial and temporal resolution are anticorrelated and there is an actual limit which is improving over the years, as shown in the literature.^[3]

The composition of a material and the size of a sample to be analysed are crucial when selecting the appropriate photon energy for measurements. Thus, the ideal sample form is

cylindrical, but there are no special restrictions for its shape or aspect ratio beyond trivial handling requests. A higher energy should be used for most metallic materials than for biological materials with high and low atomic numbers, respectively. Usable X-ray energies typically range from 10 to 120 keV at synchrotron sources,^[60] and can be up to several hundred keV at certain, dedicated high energy beamlines and for laboratory X-ray sources. This is the range known as hard X-rays.

2.2. Image Acquisition

Any tomographic or tomoscopic analysis starts with the reconstruction of many individual radiographs, also called projections, taken at different angles to one three-dimensional data set that represents X-ray absorption properties of a volume. In the course of reconstruction, the image quality of the projections must undergo several filtering steps. The exposure time must be adjusted to allow for good contrast and an adequate dynamic range of the image. In the case of a dynamic tomoscopic acquisition it is necessary to find a good compromise between the exposure time of individual projections, their number, and the desired temporal resolution depending on the type of analysis required.

Most photoelectric detectors have a dark current caused by thermal free charge carriers or a gain-dependent read-out noise. This can show up in a systematic component, which can be accounted for by subtracting an image taken without a beam (or an image averaged over several images for statistical noise reduction). The statistical component is usually significantly below the actual signal noise.

X-ray images of objects contain a non-uniformly distributed intensity offset superimposed over the actual image, which is caused both by X-ray beam intensity variations and inhomogeneities in single pixel sensitivity on the detector. This offset can be removed by a flat-field correction, i.e., a normalization with the acquired beam image without an object in the beam path.

Since the recording conditions can change over time, due to a change in temperature of the X-ray target in a laboratory source, instabilities of the bending magnet or monochromators, or a change in the number of electrons in the synchrotron storage ring, etc., and the flat-field images are usually recorded only once before or after a tomography measurement, it is useful (especially for longer recordings) to normalize the individual projections within a series of measurements with respect to the background. For this purpose, the object to be examined should be smaller than the field of view and a normalization area of the detector should be selected through which the sample never passes during stage rotation, although a flat field image in local tomography mode can also be obtained by homogenising the sample absorption.^[61] Another approach is to normalize the projections by using eigen flat fields, calculated from a principal component analysis on a set of acquired flat fields.^[62] For short measurements at stable sources, however, such corrections may be not necessary.

Other typical sources of artefacts occurring in the image reconstruction are defects in the acquisition system, e.g., dead or non-linearly responding pixels of the detector or dust particles and scratches on the scintillator that give rise to rings in the

reconstructed image. These can be partially removed during flat-field correction, but usually require a special treatment that filters lines on the sinograms in various ways or applies filters to the already reconstructed slices.^[63,64] A hardware-based approach to reduce ring artefacts is to acquire several tomograms by slightly displacing the detector to average out local characteristics.^[65]

Any material with a high absorption contrast may create artefacts in the tomographic reconstruction due to the beam hardening effect,^[66] which is a serious problem usually countered by the correction method introduced by Herman in 1979.^[67] Beam hardening, especially by metallic constituents, leads to the so-called metal artefact.^[68]

Coherent radiation produces interferences at interfaces between phases and leads to intensity fluctuations. For coherent X-ray sources such as synchrotron facilities, the projected phase images obtained from the measured interference patterns must undergo a phase-retrieval step. For this procedure, several efficient open-source algorithms and tools are available (HoloTomoToolbox,^[69] ANKPhase,^[70] Paganin^[44]). Although, strictly speaking, Paganin's algorithm only applies to single-phase systems and monochromatic radiation, it does lead to a considerable increase in contrast, and due to its ease of implementation (one only needs the image that has already been taken and one only has to select an optimal propagation distance), it is very often used. Moreover, Paganin's algorithm is the most suitable for tomography.^[71]

The determination of the correct centre of rotation is crucial, especially when recording time series of tomograms, since even small deviations of its value can be noticed in reconstructions when working with continuous exposures of successive 180° ranges. The centre of rotation should always be adjusted by viewing successive reconstructions. It is also possible that the centre of rotation changes over time, for example, due to thermal expansion in experiments at higher temperatures. Wobbling during the measurement caused by the hardware must be avoided as well, as it will lead to an imprecise reconstruction.

2.3. Spatial Resolution

Flat panel detectors usually cover an area of several hundred mm², whereas the camera chips often used at synchrotron beam lines are an order of magnitude smaller, but often have a similar number of pixels. In laboratory scanners, the enlargement of the area to be imaged is rather freely adjustable by changing the source-to-object-to-detector distances in a fan or cone beam geometry. In addition to the pixel pitch of the detector, the size and quality of the source focus has a direct influence on the maximum achievable local resolution. When using an unfocused near-parallel beam from a synchrotron source, the resolution is usually in the micrometer range^[17] and determined by the optics^[72] between the scintillator crystal and the camera, among other factors. Higher spatial resolutions below 100 nm can be obtained with nanotomography by focusing the X-ray beam using X-ray optics such as K-B mirrors or zone plates.^[73] Although such high spatial resolutions usually limit the temporal resolution considerably some recent developments allow for relatively fast acquisition times down to 6 s per tomogram under

ideal conditions.^[74,75] Laboratory nanotomography setups use nanofocus X-ray sources combined with large geometrical magnifications or a capillary condenser with an objective zone plate and a phase ring, as well as high-resolution detectors, but at the cost of temporal resolution.^[76] In the best case, the real spatial resolution corresponds to roughly twice the pixel size.

2.4. Temporal Resolution

Tomography evolves to tomoscopy whenever the achieved time resolution allows for time-resolved in-situ (or operando) measurements. There are two standard approaches when acquiring a tomoscopic series. Either successive tomograms are recorded as fast as possible with camera data transfer to the measurement computer between each tomogram, or projections of the rotating object are recorded continuously and stored in the camera cache memory until it is full. The former approach is slower and interrupts the measurement but has the advantage of using storage space on hard disks economically, having larger selectable fields of view (FOV) and larger total recording times. In addition, possible motion blurring within a tomogram is reduced as much as possible, which, however, can lead to interrupted motion if there are large time intervals between the scans. The latter approach allows for higher temporal resolutions without an interruption period, but at the cost of a reduced FOV and shorter total recording time due to the limitation of cache memory sizes in high-speed cameras. As the amount of data to be transferred from the camera in the continuous recording mode is often too large for the standard camera caches, a fast transfer and direct recording to hard disks can be beneficial as, for example, it is offered at the Tomcat beamline, SLS, and PSI.^[77]

Alternative methods to overcome limits of time resolution are available. Dynamic repetitive events can be measured stroboscopically, as Schwyn et al. and Walker et al. were able to do when studying the rapid flight motion of a fly.^[78,79] In addition, the sliding window or incremental reconstruction method can artificially reduce the time gap between two tomograms and can be sometimes useful, for example in systems where events occur on different time scales.^[2]

2.5. Tomographic Reconstruction

Tomographic reconstructions apply analytic or iterative mathematical methods to obtain greyscale single slices from X-ray projections. The entity of slices stacked together represents a 3D replica of the real sample with their greyscale values corresponding to the absorption coefficients of each constituent. Reconstruction is based on the inverse Radon transformation.^[80] Several practical reconstruction algorithms have been developed such as the filtered back projection (FBP), gridrec, SIRT or SART algorithms. Open source toolboxes such as ASTRA,^[81] TIGRE,^[82] or TomoPy^[83] are available to perform image reconstruction and processing. Furthermore, commercial software packages like Octopus, X-AID, etc. are available. Other beam geometry configurations such a fan beam (e.g., in airport X-ray tomography scanners),^[84] or a cone beam (e.g., in laboratory X-ray CT scanners) are first transformed to the parallel beam geometry, for example through the FDK algorithm,^[85] and then reconstructed. New and

more advanced methods are interlaced reconstruction,^[86–88] incremental reconstruction^[2] or artificial intelligence supported methods.^[89] Two good examples for that latter are TomoGAN^[90] and Noise2Inverse.^[91,92]

2.6. Quantitative Analyses

Besides gaining qualitative information about the structure of objects and generating appealing 3D rendered and colourful images, tomography offers to describe and evaluate characteristic parameters of the bodies under study quantitatively.^[4] A tomographic 3D volume data set is a digital twin of the sample and allows us to apply a plethora of 3D image analysis methods to extract information of all kinds. Some basic steps available for 2D images can be applied in 3D as well, include denoising, sharpening, Gauss, mean or median filtering as well as binarisation, watershed and segmentation steps. Quantitative information about certain objects can be global or local. Open-source software like ImageJ/Fiji,^[93] Python based packages like scikit-image,^[94] SPAM^[95] or 3D Slicer^[96] or commercial packages such as Avizo/Amira, VGStudio, Dragonfly or MATLAB have different quantitative add-ons and are available on the market.

Time-resolved measurements as obtained when performing tomoscopy open a new dimension for analysis. Characteristic parameters can vary over time during sample structure evolution. 3D image filters and other volume treatment procedures have to be implemented as well as temporal filters. The integration of temporal evolution into image processing leads to a considerable increase in the demand for computing power. One example is Tofu, a toolkit for reconstructing, processing and analysing large volumes of images.^[97] Furthermore, new methods based on artificial intelligence may support analyses and speed up the computations in the future even more.

2.7. Competing Parameters

In in-situ experiments, tomography allows us to gain more information about the evolution of a system, but often at the expense of spatial resolution. It is well known in the imaging community that spatial and temporal resolution are interrelated.^[98,99] One can improve one by decreasing the other, similar to what is the case in fast X-ray radioscopy experiments.^[98,100] Villanova et al.,^[101] Yashiro et al.^[102] and García-Moreno et al.^[3] as well as the Tomoscopy Experiments database^[52] show that there is a limiting boundary for both. Figure 2 shows that there is a limit for temporal resolution, which has improved almost exponentially over the past years.

In a successful experiment, a compromise must be found between various tomographic settings based on the expectations given by the background of the experiment. In order to avoid blurring of the tomograms and depending on the evolution of the fastest features in the system, it is recommended to fulfil the criterion

$$v_{\text{evol}} \leq \frac{x}{t_{\text{tomo}}} \quad (1)$$

which serves us as an estimate of the permissible velocity v_{evol} of a feature for a given pixel size x and time for one tomogram

Table 1. Data acquisition parameters used for recent experiments performed at the tomcat beamline, PSI and presented recently.^[3]

Experiment	Exp. 1	Exp. 2	Exp. 3	Exp. 4	Exp. 5
Pixel size [μm]	2.75	2.75	2.75	2.75	2.75
Temporal resolution [tps]	50	200	400	650	1000
Number of projections	200	100	100	62	40
Exposure time [ms]	0.02	0.02	0.02	0.045	0.09
Field of view [mm^2]	3.05	1.12	0.51	0.46	0.48
Experimental time [s]	72	59	23.8	68.2	43.9

t_{tomo} .^[2] However, a variety of other parameters such as spatial resolution, image contrasts, etc. has to be taken into account to ensure the quality of reconstruction. There are no general criteria because the quality of the tomograms has to be just good enough to answer a given scientific question, which depends on the level of analysis requested, and this can vary between different studies.

Besides spatial resolution and temporal resolution, we consider four more parameters, namely exposure time of a single projection chosen such to ensure a sufficient dynamic range of the images, field of view (FOV), number of projections (depending on FOV) and duration of experiment. Since it is difficult to obtain all the required information from other groups, these six parameters were taken from various benchmark experiments that we conducted as part of our recent work and are summarized in **Table 1**.^[3]

Figure 3 shows a radar plot that evaluates six competing parameters of several experiments that we have performed.^[3] For simplicity we use pixel size and tomogram acquisition rate as a rough measure for spatial and temporal resolution, respectively. With a proper calibration of the plot, the maximum area inside each parameter line should quantitatively characterize a certain experimental setup and denote its performance capability. Readjustments of the parameters are possible, for example if only a short measurement time is requested, but inside the limits giving by the largest area, i.e., by the setup. Qualitatively we can observe in **Figure 3**, that an increase in temporal resolution implies a mandatory change of other parameters.

3. Results

Tomography as a method to study engineering materials such as, for example, casting alloys or aluminum foams started being widely applied around the year 2000.^[21] Some of these materials are still the focus of today's research, albeit with new research perspectives. In the past, investigations concentrated on the evaluation of structural features in solid samples. For the analysis of dynamic processes in the μm -range and at high speeds, time-resolved tomography has continuously developed over the last decades. An overview of the development of temporal resolution since 1995 for various published experiments at different facilities has been given in the literature^[101,103] and is summarised in **Figure 2**. The benchmark has moved from 260 s for a single tomogram in 1997 to one millisecond acquisition time per tomogram in 2021,^[2,3,60,101,104–109] the latter corresponding to a

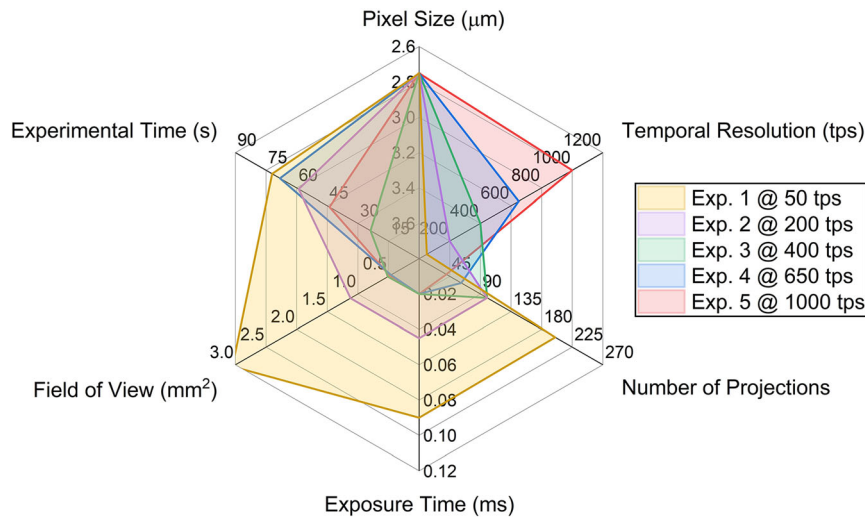


Figure 3. Radar plot showing the dependence of six competing parameters as they were selected in several experiments performed at the Tomcat beamline, PSI and presented in a recent work.^[3]

temporal resolution of 1 ms.^[3] This progress, which implies an increase of average scanning rate by an order of magnitude every four years, has been enabled by the development of synchrotron radiation sources, camera sensors, optics, data processing capacities, storage rates, etc., and has opened the door to specialised quantitative three-dimensional analyses of fast dynamic processes that were not possible a decade ago. Recent developments have focused on in-situ, operando and multi-method approaches for the analysis of dynamic processes instead of simple static measurements. As a consequence, sample environments become more a crucial factor for success, but at the same time sample handling becomes more challenging due to the high rotational speeds required. As an example, samples have to be very well fixed and centered, or be placed tightly in an X-ray transparent holder, to avoid them to fly away. In most cases, obtaining the highest spatio-temporal resolutions with large fields of view and long total acquisition times is not possible and compromises have to be sought. For example, an improvement in tomographic acquisition rate can be achieved at the expense of spatial resolution.^[2,101] A suitable experiment with a good temporal resolution can only be achieved after finding a compromise between different acquisition parameters such as pixel size, field of view, exposure time, number of projections per tomogram and total number of tomograms. The optimisation of these parameters always depends on the experimental conditions and research objectives, see Figure 3.

The following case studies provide an exemplary overview of the latest research topics in the field of tomography and tomography application to metallic materials. Most of the examples shown here have a time dependence that not only reflects the evolution of the sample structure, but also permits insights into the processes involved. Recent reviews take this trend into account and focus more on time-dependent studies.^[4,17,88,102]

3.1. Mechanical Performance

When selecting a structural metal-based material, mechanical performance is the most important property to consider, along

with the cost.^[110] Research is often focused on understanding the performance of metallic materials by relating their microstructure to their mechanical properties and explaining the mechanisms of mechanical behaviour. X-ray tomography offers a non-destructive way to analyse microstructures, allowing for series of tests to be performed on the same sample subjected to different treatments. In the simplest case, ex situ sample treatments are carried out and measurements of the same sample are taken at different stages. For example, a sample was exposed to fatigue testing and periodically monitored with tomography^[111] or quasi-statically deformed on a testing machine and re-measured after each step in the tomographic setup.^[112] A more sophisticated possibility is an in-situ analysis with a special experimental setup that allows for an interrupted tomography scan after each sample handling step without removing the sample from the tomographic stage.^[113] A logical further development has been in-situ dynamic tests provided that the acquisition rate is high enough. For example, Maire et al. performed dynamic deformation experiments showing failure and fracture of an aluminum-based metal matrix composite at 20 tps.^[109]

Some of the tomographic studies on metals have focused on topics related to quasi-static defect evolution,^[114–119] corrosion,^[120] fatigue cracks,^[115–117,119] diffusion^[121] or hardness^[76] for which the spatial and temporal resolution is usually not very high. Other studies deal with sintering of metals powders.^[122]

Sintered metallic fibres find application as implants, catalysts or heat exchangers.^[123] **Figure 4** shows AlSi fibres used for high-performance heat exchangers before and after liquid phase sintering. Sinter contacts of considerable size appear already within 5 min after the sample has reached the sintering temperature of 600 °C. Furthermore, gas bubbles evolving inside the fibres were found, which has to be avoided to preserve their mechanical performance.

3.1.1. Mechanical Properties

X-ray tomography has been used to study the evolution of defects mainly in Al, Mg, steel and Ti alloys among others. Maire et al.

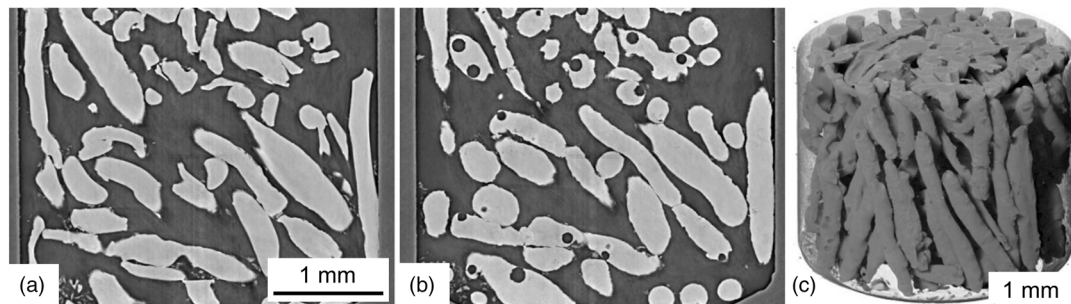


Figure 4. In-situ tomography analysis of liquid-phase sintering of Al-Si fibres, a) before and b) after sintering at 600 °C. c) 3D rendered view of the sintered condition. (Al-Si fibres kindly provided by Olaf Andersen, Fraunhofer IFAM Dresden).

reported investigations of damage in aluminum alloys,^[124] deformation mapping and damage accumulation conducted by X-ray tomography.^[4] Karagadde et al. observed transgranular liquation cracking of grains in semi-solid AlCu15^[125] while Puncreobutr et al. studied the defect evolution in the same alloy in a quasi-static configuration^[114] as well as the evolution of voids and of the strain map by hot tearing as shown in **Figure 5**.^[126] Other groups focused on the analysis of crack development induced by pressure^[115] or fatigue.^[116] Recently, Wicke et al. studied fatigue crack propagation in the commercial aluminum alloy EN-AW 6082,^[119] Xue et al. in titanium^[117] and Junet et al. in TiAl6V4.^[118] Tomography played a central role in all these works.

3.1.2. Porosity in Metals

Porosity affects the mechanical performance of metals in terms of reduced strength and fatigue resistance and can cause parts to

fail. It also contributes to the reduction of corrosion resistance and to an inferior weldability. The porosity of a sample is defined as the ratio of the volume of all voids to the total sample volume. Reducing porosity has always been an important challenge for any casting or welding process. Modifications of pressure die casting procedures or post-compression of already solid parts to partially close the porosity have only limited success.^[127] Therefore, researchers try to understand and counteract porosity formation mechanisms. For this challenge, X-ray tomography has been a very useful tool in materials science in recent years. Such studies are facilitated by the very high X-ray absorption contrast existing between pores and any metal matrix.

Buffière et al. investigated the porosity of AlSi7Mg alloy and its influence on the development of fatigue cracks^[128] as well as Maskery et al. on additively manufactured AlSi10Mg alloy,^[129] Tammam-Williams et al. on additively manufactured titanium,^[130] while Liu et al. in TiAl6V4^[131] and Babout et al. analysed porosity

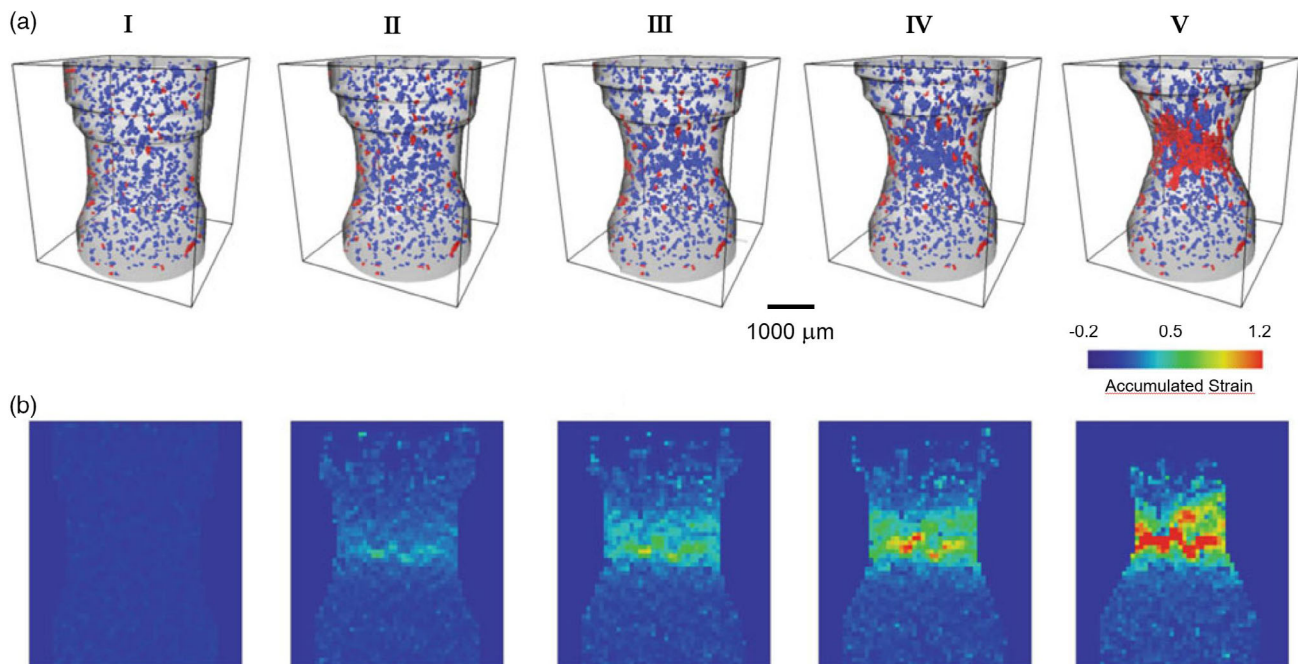


Figure 5. a) Rendered 3D volumes and b) strain map of an AlCu15 alloy during solidification. Nucleation of voids, void growth and coalescence during hot tearing can be observed. Reproduced with permission.^[126] Copyright 2013, Springer.

in metal matrix composites.^[132] De Giovanni et al. quantified the porosity in strontium modified Al-Si alloys^[133] and Mukherjee et al. the microporosity in Al-Si-Cu foams.^[134]

3.2. Structure and Microstructure Evolution

16 million tonnes of aluminum castings were produced worldwide in 2020.^[135] Knowledge describing the formation of cast microstructures, which ultimately determine mechanical properties, is crucial for further improved product quality. In the past decade, insightful studies have been carried out using tomography and tomography. Most notable works include studies of the solidification of aluminum alloy,^[136–141] formation and evolution of microporosity,^[142] nucleation and growth of intermetallic phases,^[143,144] morphology of dendrites and their evolution over time,^[142,145–150] cellular-to-dendrite transitions,^[151] remelting^[152] or coarsening in the semi-solid state.^[153,154] Tomography has also contributed to the confirmation of theoretical models, phase-field or multi-scale simulations of the microstructure evolution in solidifying metals.^[149,150,154–156]

3.2.1. Solidification Structure

The majority of in-situ solidification studies were carried out on Al-Cu or Al-Ge alloys, which are considered reference systems and convenient model alloys as both copper and germanium offer a high X-ray absorption contrast to aluminum compared to silicon in common Al-Si casting alloys, but also in commercially available alloys such as A319 (Cu containing Al-Si alloy).^[114] Other metallic alloys have been studied, e.g., Yang et al. imaged the dendrite morphology of Mg casting alloys,^[155] Guo et al. that of Mg-Zn alloys,^[157] Subroto et al. the solidifying behaviour of MgNd5Zn5^[158] and Azeem et al. dendrite formation in Fe, Co and Ni alloys at high temperatures.^[159] Solidification studies have also been carried out on other metallic structures using tomography. For example, Mukherjee et al. observed defect generation during solidification of AlSi6Cu4 metallic foams.^[160]

During solidification of the widely used Al-Cu alloys, a complex mixture of primary dendrites and lamellar eutectic forms. The eutectic is influenced by tiny additions of modifiers such as sodium or strontium. The ever-present impurities (Fe and Mn) lead to the formation of intermetallic phases. Such coupled phenomena have been studied in-situ by X-ray radiography.^[139,161–165] The method is fast enough to elucidate the formation of phases during solidification, but limited to thin samples to avoid many morphological features to be superimposed in the X-ray projection images. In this case, solidification artefacts caused by crucible walls and surface oxides might have an impact on such experiments that are hard to assess or control. Radiography provides impressive images of dendrite growth,^[139,161,162] even under microgravity,^[166,167] but comparison of the obtained pseudo-2D data with models^[165,168,169] shows limitations despite some recent progress.^[170] Although it has been shown, for example, that fractured dendrites cause a transition from columnar to uniform growth or that concentration profiles can be derived at the solid-liquid interface, the potential for deriving 3D information from 2D data is limited, thus limiting the possibilities of a detailed quantitative assessment.^[171]

Tomography solves the problem of overly constrained samples and image overlap but has been too slow for a long time to be used at realistic cooling rates and has been mostly applied to ex situ analysis of samples in which solidification was interrupted by quenching,^[148] under isothermal conditions^[147] or at very low cooling rates.^[144] An example for the latter case is given in **Figure 6**, where the formation of intermetallic phases during slow cooling is given with a temporal resolution of 1 scan per minute.^[144] Similar temporal resolutions have been also used in the work of other groups.^[143]

Maire et al. quantitatively characterized intermetallic phases in an industrial AA5182 alloy^[172] and Cai et al. the granular and intragranular deformation during compression of an equiaxed dendritic Al-Cu alloy in the semi-solid state.^[173] Puncreobutr et al. studied the influence of Fe-rich intermetallics on solidification defects in AlSiCu alloys^[174] and Shahani et al. the eutectic growth in Al-Ge alloys at a rate of 1 tomogram each 30 s (0.033 tps).^[175]

In-situ tomographic experiments with a notably higher temporal resolution were performed in 2005 by Ludwig et al. at 0.1 tps to study grain formation in AlCu4 alloys.^[176] Almost a decade later Cai et al. studied the transition from cellular to dendrite growth at 0.2 tps,^[177] Puncreobutr investigated the solidification structure and defects, the evolution of intermetallic morphology and the development of damage during hot tearing of Al-Cu alloys at 0.5 tps^[178] and Gibbs et al. analysed the morphology of growing dendrites in an AlCu24 alloy at a rate corresponding to 1.8 s per tomogram.^[179] A few years later Daudin et al. examined particle-induced dendrite modifications in the commercial aluminum alloy AA 6082 with a time resolution of less than 1 s^[180] and monitored the formation of dendritic morphology at 3 tps.^[181] Although in 2012 a higher time resolution of 6.6 tps was reported by Salvo et al., who studied the kinetics of growth of the solid phases in Al-Cu alloys at cooling rates up to 4.9 K s⁻¹,^[140] most of the work to date have not fallen below the 1 tps barrier. Recently, the present authors have applied higher tomography rates of hundreds of tomograms per second to exploit new possibilities in studying the microstructure evolution of alloys solidified at typical industrial cooling rates of up to 20 K s⁻¹.^[3] In these experiments, AlGe10 alloys were melted in a rotating boron nitride crucible using IR lasers, cooled down and solidified in a controlled manner while recording tomograms continuously. Formation of dendrites was shown, and their tip velocity calculated based on data acquired at 200 tps, see **Figure 7**.

3.2.2. Solidification Porosity

Whenever alloys solidify, porosity is near. The primary reasons are the shrinkage of the alloy during solidification (in aluminum by $\approx 6.5\%$ in terms of volume) and the influence of gases involved. The solubility of hydrogen drops by almost 95% during solidification and excess hydrogen precipitates in pores. Moreover, any gas involved in the casting process (for example air, steam or gaseous residues from the mould) is likely to be entrapped in pores. Depending on the type of alloy and the temperature gradient in a casting the mechanism of porosity formation varies and the resulting porosities show a wide range

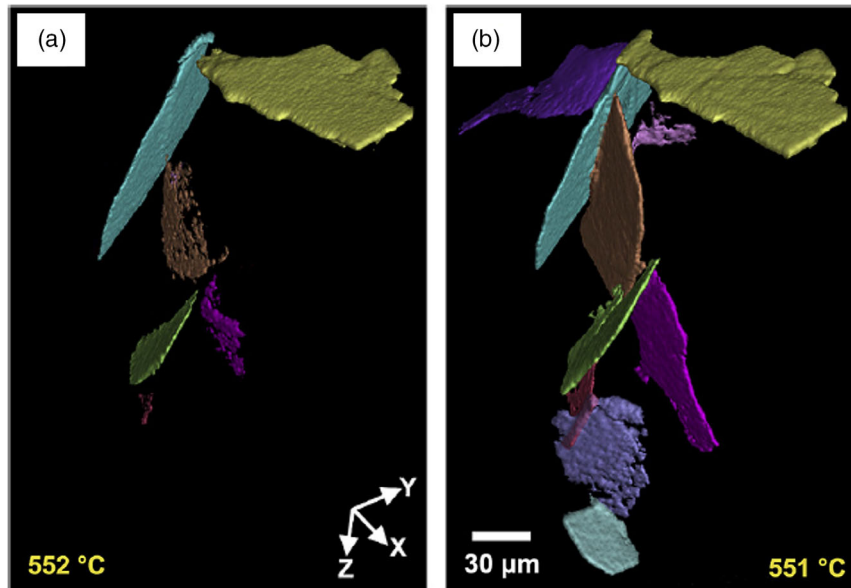


Figure 6. Growth of the δ -phase during solidification of AlSi10Fe0.3 alloy. Changes within a minute upon cooling by 1 K are shown in a) and b). Each colour represents an independently grown plate. Nucleation and growth are very fast. Reproduced with permission from Elsevier. Reproduced with permission.^[144] Copyright 2017, Elsevier.

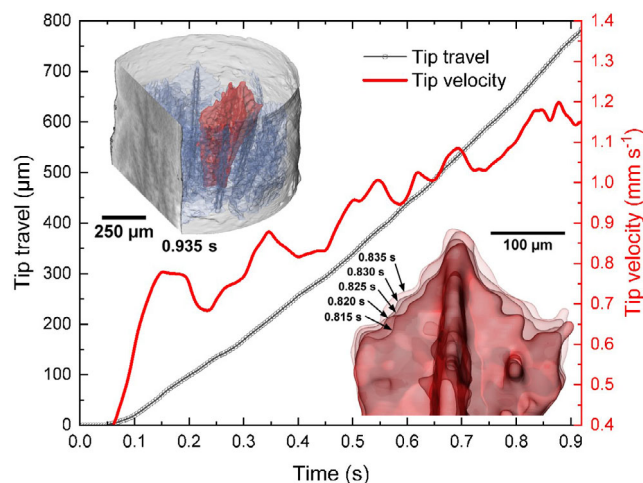


Figure 7. Tomoscopy of the evolution of aluminum dendrites in AlGe10 alloy during solidification at a cooling rate of 17 K s^{-1} recorded at 200 tps and quantitative analysis of the travel distance and velocity of the tip. The insets show a selected rendered Al-rich dendrite and its evolution as overlapping tomograms during several 5 ms intervals. Reproduced under the terms of the CC-BY license.^[3] Copyright 2021, The Authors, published by Wiley.

of morphologies. Tomography is an ideal tool to study such phenomena.

Solidification can give rise to porosity such as surface defects or internal defects such as hot tears or blowholes whenever the feed of liquid to the final solidification region is restricted and cannot compensate the volume shrinkage of the solidifying melt.^[182] Solidification porosity is found in many cast metal components, but is particularly common in aluminum and magnesium die castings.^[183] In die casting air is entrapped in the

solidifying melt due to the turbulence created by rapid melt displacement.

The formation of solidification porosity in AlGe10 alloy has recently been investigated in situ using X-ray tomography at a rate of 50 tps. **Figure 8** shows a tomogram extracted from a time-resolved series which distinguishes different types of porosities, namely gas porosity given in blue and shrinkage porosity in red.

The formation of porosity is also influenced to a large extent by the velocity of the solidification front. A relevant example of this dependency is the rapid cooling during powder bed welding,

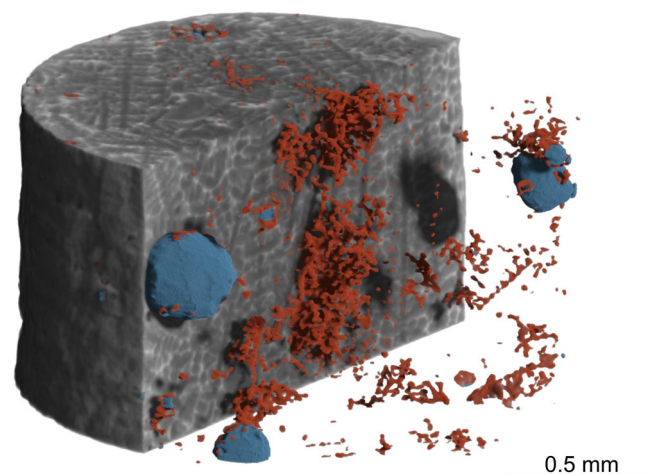


Figure 8. AlCu10 sample solidified at 5 K s^{-1} studied in situ with X-ray tomography at a rate of 50 tps. The dendritic alloy is given in grey while different types of porosities are coloured: Gas porosity corresponds to 0.9% of the volume (in blue) and shrinkage porosity to 0.6% (in red). The classification was made according to the morphology.

similar to welding. Locally melted areas solidify very fast, so that the dissolved gas has little time to diffuse out. De Plessis et al. reviewed the effect of porosity on mechanical properties in alloys processed by additive manufacturing through X-ray tomography. Some other works addressed the influence of porosity in TiAl6V4 alloys produced by wire arc additive manufacturing^[111] and with laser powder bed fusion.^[131]

3.2.3. Metals in Minerals

In geology and mineralogy tomography is used on a routine basis. For example, researchers have studied the distribution of metals in minerals and how they can be extracted. Francois et al. demonstrated that in-situ X-ray tomography has the potential to link fracture fundamentals and ore texture characteristics by analyzing a quasi-static, tensile-activated rock fracture, triggering the failure and fragmentation of a copper ore.^[184] They describe the pressure dependence of failure and fragmentation, as shown in **Figure 9**, with the aim of finding a way to extract metals efficiently. This knowledge can help in designing optimal processes for critical mineral release and provide valuable data for modelling.

3.3. Metal Foams

Unlike in conventional casting, where avoiding porosity is of paramount importance, cellular metals contain a high fraction of open space deliberately created in order to create materials with a novel spectrum of properties. Such cellular or porous metals have a legitimate application potential, similar to polymer foams.

Many manufacturing routes have been designed for producing cellular metallic structures, and one route is to foam a metal or alloy.^[185,186] Here, the term foam refers to a state in which a largely disordered arrangement of bubbles or cells is distributed in a liquid or solid matrix. A liquid foam is usually a transient state leading to a solid foam. We can distinguish between closed-cell and open-cell metal foams, both having a wide range of applications stemming mainly from their mechanical and functional properties.^[187] Close-cell metal foams are produced following either the powder metallurgical route or the melt route,^[186] while open-cell foams are made by modifying close-cell foam after foaming or by coating a polymeric precursor.^[188] Using space holders^[189] or replication^[190] methods is another option to manufacture a more general class of cellular structures that differ from foams by their morphology.^[185] In recent years, metal foaming technology has been commercialised on a small scale.^[187] The quality and properties of a final solid foam are determined already by the structure of the evolving liquid foam precursor. The stability of liquid metal foams is ensured by dispersed solid particles such as SiC or resident oxides contained in the original metal powders.^[191–194] The stabilisation process is very complex and the in-situ observation and X-ray tomography analysis of the liquid foam development is a great opportunity for improvement.

3.3.1. Mechanical Properties

Metal foams, and especially foams made of aluminum alloys, have been examined with X-ray tomography for a long time.^[5,195–197] Primarily, the mechanical properties under

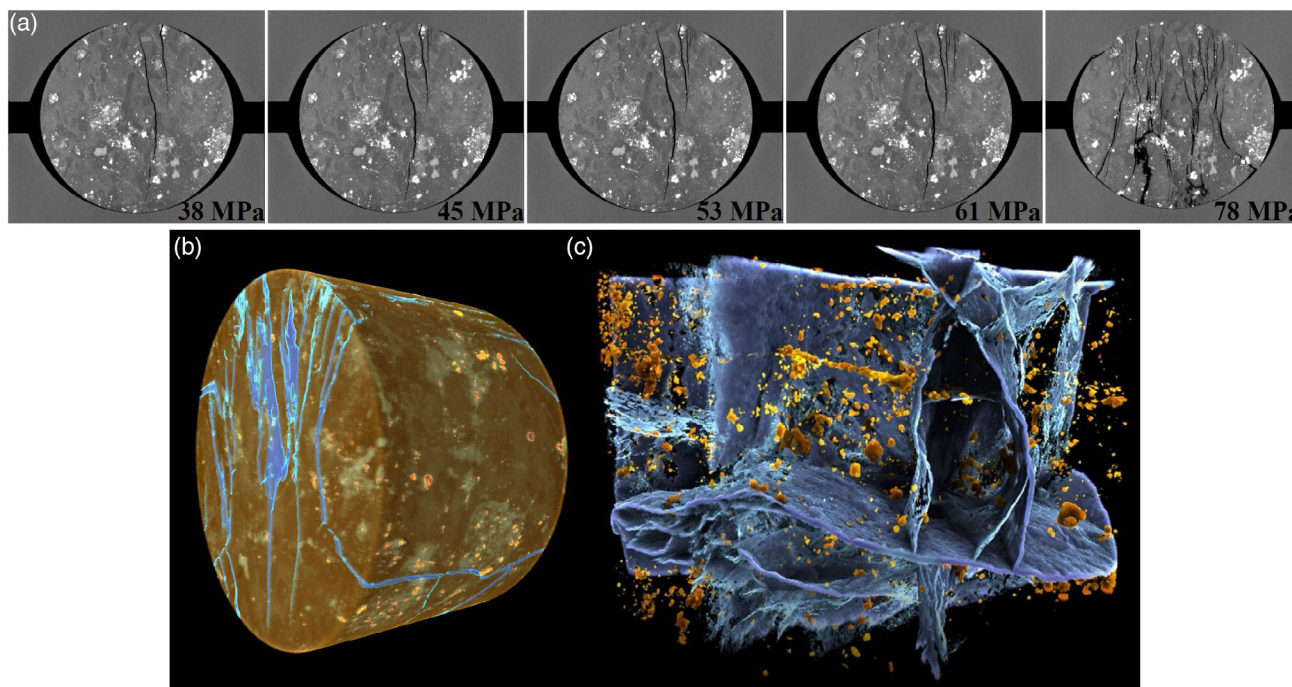


Figure 9. a) Tomographic cross-sections showing the successive fracture and fragmentation of ore (rock diameter = 12 mm). b) 3D rendering of the fragmented ore. Fractures are highlighted in blue and Cu-rich minerals in orange. c) 3D rendering of the fracture network and the Cu-rich grains. Reproduced under the terms of the CC-BY license.^[184] Copyright 2022, N. Francois.

uniaxial loading were investigated in conjunction with the cell structure.^[112,198] Islam et al. studied the microstructural and mechanical properties of cell walls of closed-cell aluminum alloy foams^[199] and the mechanical response under dynamic load.^[200] Kolluri et al. researched the effect of fatigue on constrained aluminum foams.^[201] Kang et al. produced and studied the mechanical properties of open-cell austenitic stainless steel foams.^[188]

Recently Wang et al. studied the performance^[202] and the deformation behaviour^[203] under compression of aluminum alloy foams produced by the melt route. By analysing the deformation of single cells, it was possible to predict which cells are more prone to collapse during subsequent compression, as shown in **Figure 10**.^[203] In a further study, a short-range order of monodispersed cells in foams produced by the melt route with a special gas injector was discovered and described.^[204] Girolamo et al. investigated the correlation between morphology and compression behaviour^[205] and Neu et al. for the specific case of aluminum foam sandwich panels.^[206] X-ray tomography was also used as an input for thermal^[207] or electrical^[208] conductivity analyses in metal foams as well as for finite-element simulations.^[209] With high spatial resolution, Luksch et al. studied the microstructural damage behaviour of individual struts in open-cell aluminum foams, whereby the influence of primary inclusions became clear, as also shown in **Figure 11**.^[210]

3.3.2. Foaming Process

In addition to the investigation of solid samples, tomography has also been used to investigate the influence of production parameters on the manufacturing process through in-situ experiments e.g., to study the effects of reduced^[211] and high ambient pressure^[212] on the evolving liquid metal foam structure, or the influence of the blowing agent content.^[212] Mukherjee et al. performed a deep analysis of microporosity formation,^[134] the effect of cooling rate after foaming on the resulting cellular structure,^[213] defect generation during solidification^[160] and foam collapse,^[214] while Jiménez et al. analysed the positive effect of vacuum powder compaction on the foaming behaviour^[215] as well as the foaming process in a multi-method approach, simultaneously combining tomography with X-ray diffraction and optical measurements of foam expansion.^[216]

In-situ X-ray radiography has in the past helped to understand the growth and coalescence of bubbles^[217,218] or the stabilisation

of liquid metallic films and metal foams^[193,194] and has suggested ways to improve foaming techniques. The development of bubbles (ideally spherical, uniform in size and with smooth walls) is determined by bubble nucleation and early growth that are not accessible with radiography but require tomography.

Aluminum foams (mostly based on AlMgSiCu alloys) were produced by melting compacted powder mixtures including a blowing agent in a rotating crucible using heating IR lamps or lasers. Tomograms were continuously recorded during melting and foaming. The slices shown in **Figure 12** were recorded at 50 tps and show the development of cell structure, in particular coalescence of two bubbles and the influence of this event on their immediate neighbourhood. The artefacts in the second slice show that this recording rate is too slow to observe this phenomenon in detail.

Another goal was to understand the nucleation of bubbles in detail. Their number, position, orientation and shape were extracted from the tomograms. The bubbles were individually labelled and followed throughout the foaming process with image analysis tools. When blowing agent particles (usually TiH₂) are present in the material, two-stage nucleation was observed: First, nucleation is driven by gases adsorbed to particles in the powder compact, after which it is dominated by the hydrogen gas released from the blowing agent. The two bubble populations differ in their development, which could be investigated by tracking a large number of bubbles and their shape (adsorbates produce very round bubbles while the blowing agent does not). Understanding this complex scenario and adjusting the blowing agent by thermal or chemical treatment as well as the selection and distribution of metal powder particles to achieve a uniform arrangement of bubble nuclei has been the subject of research for many years, but with limited success.^[219–222]

In addition, bubble growth was investigated. Foam ageing by gas diffusion through the cell walls or by spontaneous rupture of films can be studied at moderate tomographic rates of 5 tps. Since the volume of each bubble can be tracked, it is possible to determine which bubble collapses at which stage.

With the development of X-ray tomography and the corresponding increase in time resolution, the new possibilities offered by tomography have been applied to evolving metallic foams by the present authors.^[2,60,216,223,224] Kamm et al. observed the dynamics of the foaming process,^[224] in particular nucleation and bubble evolution in early stages as the final cellular structure of the

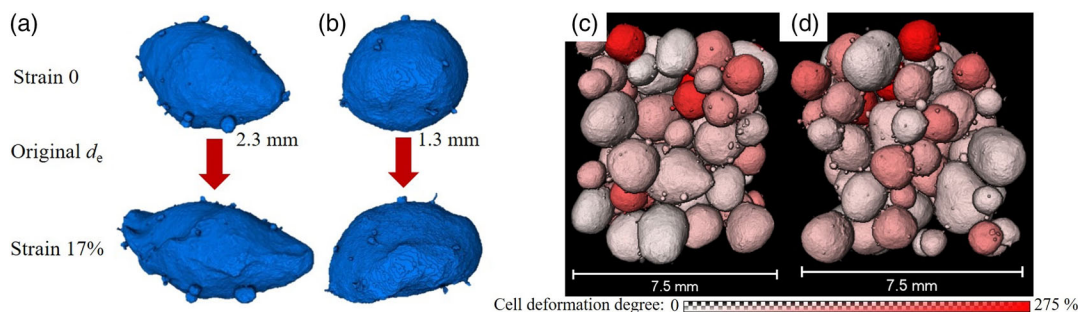


Figure 10. a,b) Two deformed cells at zero strain and 17% strain. c,d) Prediction of cells that are more prone to deform according to their degree of deformation. (c) Views from the xz plane and (d) from the yz plane. Reproduced under the terms of the CC-BY license.^[203] Copyright 2021, The Authors, published by Wiley.

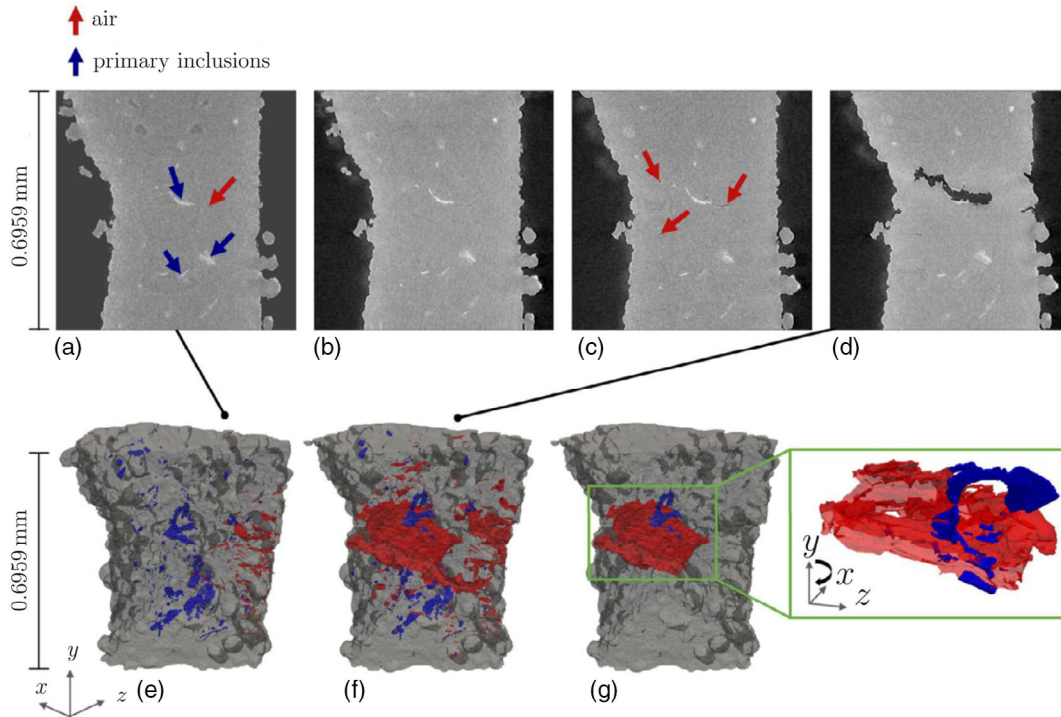


Figure 11. a–d) Slices and e–g) rendered 3D tomograms from an interrupted tensile test analysis of a strut of a metallic foam at different times. Red and blue arrows show air and primary inclusions, respectively, (a)–(d) show developing cracks. (e) Original strut without deformation, (f) and (g) after tensile deformation, the latter showing cracks in red and blue. Reproduced with permission.^[210] Copyright 2021, Elsevier.

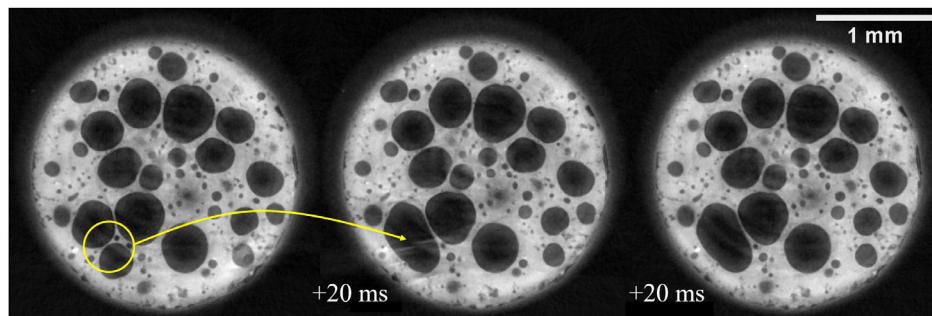


Figure 12. Tomoscopic slices of an evolving AlSi8Mg4 metal foam at 20 ms intervals and recorded at 50 tps, showing the coalescence of two bubbles and the influence on the surrounding neighbourhood. Yellow circle marks two bubbles that merge 20 ms later to the one indicated by the yellow arrow.

solid foam is dictated by the evolution and stability of its liquid counterpart.^[225] During foaming the structure coarsens mainly due to the coalescence of bubbles as a result of the rupture of liquid films separating adjacent bubbles,^[218,226] leading to an inhomogeneous foam structure, which is known to be detrimental to mechanical properties and reproducibility of such properties.^[227–229]

Recently, the current authors were able to study liquid foam evolution including fast phenomena occurring in foams such as bubble coalescence at tomographic rates of up to 1000 tps as given in **Figure 13**.^[2,3] It was shown that the liquid metallic films separating two bubbles rupture in less than 1 ms. The entire coalescence event including movements and rearrangements after rupture takes about 1.2 s before a stable new bubble in its final

shape is formed. This entire foaming process was continuously monitored in full detail at the same high acquisition rate over a period of 43.9 s.

3.4. Welding

Laser processing of metal has already reached a high level of performance and maturity and has proven its advantages in modern production. Nevertheless, engineers and scientists continue developing the process to optimize quality and cost efficiency.^[230] One example is the introduction of dynamic beam shaping using newly developed piezo-driven actuators in advanced laser optics that enable beam guidance in all spatial directions.^[231–233]

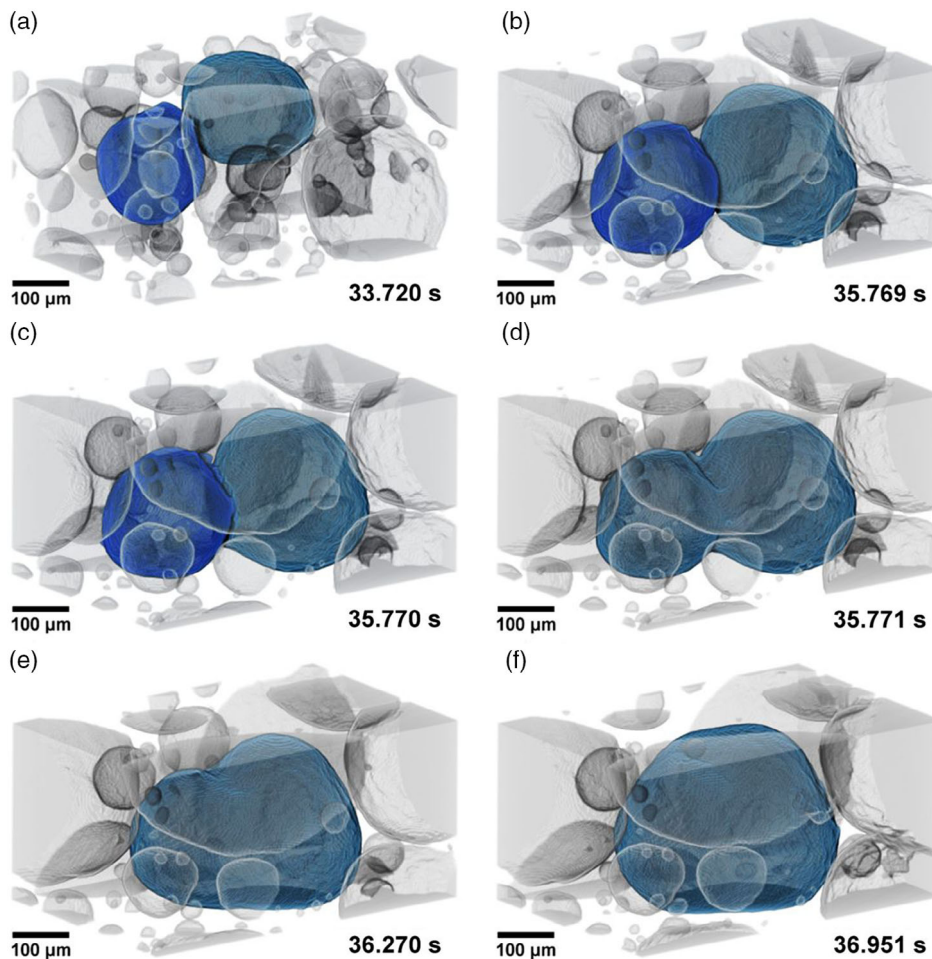


Figure 13. a–f) Rendered tomograms extracted from a tomography series of the coalescence of two gas bubbles marked in cyan and blue at ≈ 550 °C inside a liquid AlSi8Mg4 alloy foam recorded at the highest tomography rate of 1000 tps. The rupture of the film separating the two gas bubbles occurs in less than 1 ms, the relaxation of the resulting bubble is delayed over a period of ≈ 1.2 s.^[3] Reproduced under the terms of the CC-BY license. Copyright 2021, Wiley.

Historically, laser welding and cutting have had the greatest acceptance in production technology, but there are other interesting applications such as laser metal deposition, laser cladding, laser surface cleaning or hardening, etc.^[230] In recent years, laser powder bed fusion (LPBF) has experienced a significant upswing driven by the rapid development of additive manufacturing and its undeniable advantages for the production of complex metallic parts.^[234–236]

3.4.1. Porosity in Weld Seams

The quality of a weld is very important from the point of view of the mechanical properties of components but also from a safety point of view. Porosity in welds has always been a major problem in metal processing that needs to be dealt with. Porosity in metallic welds is mainly caused by gas (air or shielding gas) that becomes trapped when turbulences occur in the weld pool and the metal freezes before all the gas in the weld pool can escape.^[237,238] The gas can also come from cavities in the welded parts that are opened during welding, for example of casting alloys. Finally, hydrogen porosity can also be a contribution.

Zhao et al. held a critical instability at the moving keyhole tip responsible for porosity formation during laser melting.^[239] Fetzner et al.^[231] and Börner et al.^[233] were able to show that laser beam oscillations during welding reduce porosity in the weld seam in aluminum alloys. This has recently been confirmed with X-ray tomography, see **Figure 14**. Large pores with an equivalent diameter of 550–750 μm , which occur when standard static laser beam guidance is applied and are shown in Figure 14a,c, can be avoided by applying oscillating guidance, as shown in Figure 14b,d and quantified in Figure 14e,f, with maxima at pore sizes represented by their equivalent diameter of ≈ 50 μm . In addition, the total porosity of the seam can be reduced from 28% with static beam guidance to 21% with oscillating beam guidance.

3.4.2. Laser Welding Process

In laser welding, metallic components (often sheets made of aluminum or steel) are heated rapidly by focused radiation and a small advancing cavity, also known as a keyhole, is created. On the tail of the keyhole, solidification sets in and the parts are joined. The demand for light-weight and multi-material

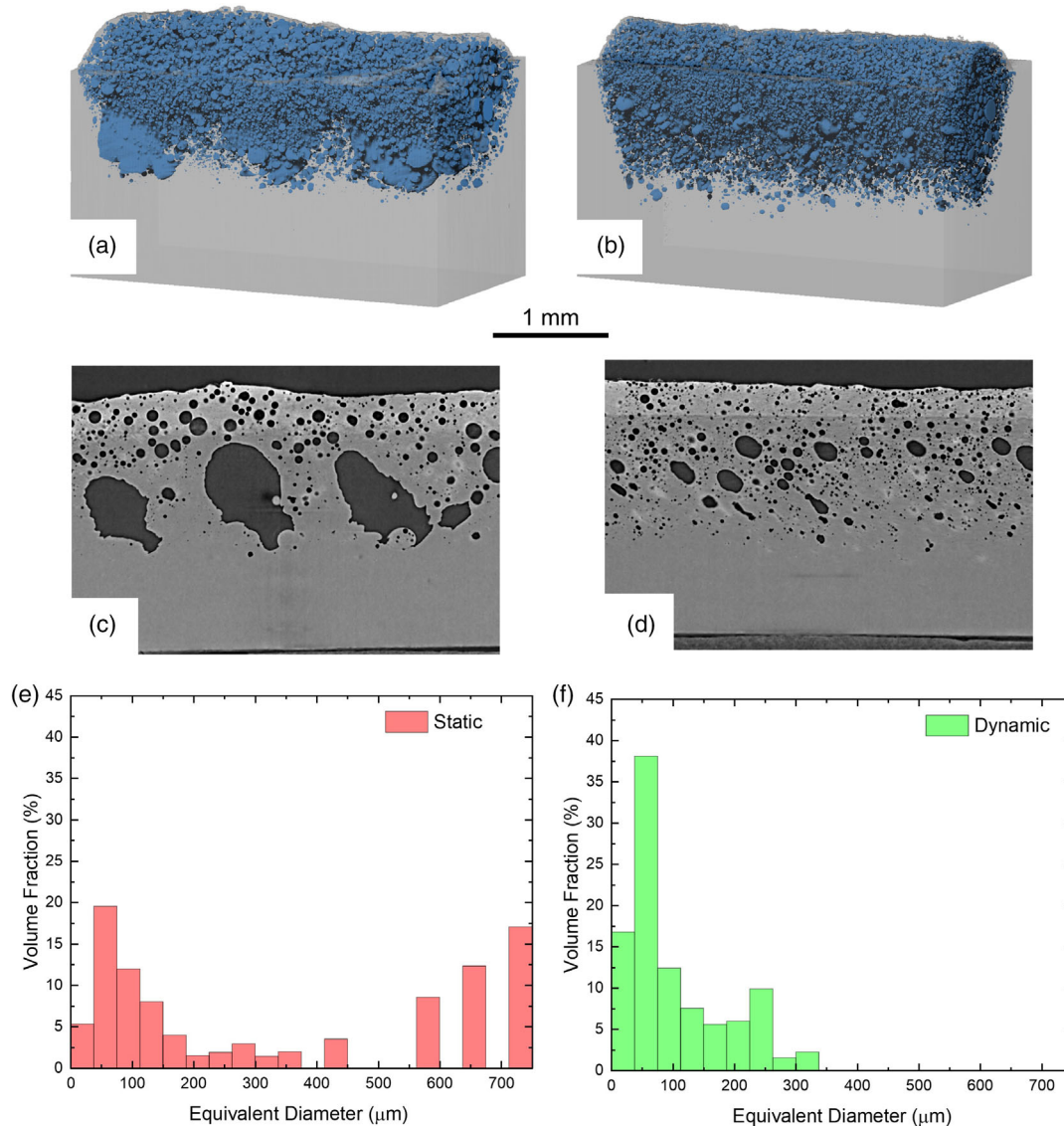


Figure 14. Tomograms of laser weld seams in an AlSi10 cast alloy. a) A wide and irregular weld seam produced by a standard static beam (28% porosity) and, b) a finer weld seam produced by a dynamically oscillating laser beam guidance (21% porosity). Tomograms were recorded after welding. The pores are coloured in blue, while the AlSi10 matrix material has been set to transparent. c,d) show slices through the centre of the seam corresponding to (a) and (b). e,f) show the corresponding equivalent pore diameter distributions of the volume-weighted porosity fraction of the weld seam shown in (a) and (b). The 3 bars at 550–750 μm in (e) correspond to the 3 large pores in (a) and (c). The quality of the weld seam produced by dynamically oscillating laser beam guidance is clearly superior.

constructions necessitates constant further development of this technology.^[240]

The processes in such welds are difficult to observe experimentally. X-ray radioscopy at up to 250 fps,^[241] 1000 fps^[242,243] or even 2000 fps^[244] has recently been used to unravel the processes in complex weld zones in situ during welding, however, with the usual limitations of radioscopy. As X-ray tomography is now available at high acquisition rates, investigations have been started to study welding in-situ also in 3D.^[3] Börner et al. investigated keyhole formation during laser welding at realistic welding speeds of 1 m min^{-1} and studied the processes involved such as metal displacement, pore formation or metal flow.^[233]

A special variant of laser welding was studied in which a small-amplitude oscillation of the laser beam is superimposed on the general linear feed of the beam. The beam motion and oscillation were generated using a programmable positioning system of the laser. The investigation showed how the oscillating beam is beneficial compared to the standard static beam guidance. Börner et al. also used X-ray tomography for the first time to prove the concept. The constant rotation of the sample as required by tomography and the beam positioning were synchronised such that the keyhole advanced along a circle of 2 mm diameter at the selected velocity of 1 m min^{-1} in the reference system of the rotating sample. First results are shown in Figure 15.^[233]

There a circular weld seam between a wrought aluminum alloy pin (1) and a die-cast aluminum alloy ring (2) is shown for the case of a standard, static beam and an oscillating beam guidance, last producing a more homogeneous seam with less metal ejections. A detailed analysis is in preparation.

3.5. Additive Manufacturing

X-ray tomography is increasingly recognised to be a method that can help to improve manufacturing processes in materials engineering.^[245] One current topic is additive manufacturing (AM) of metallic materials.^[234,246,247] The potential to contribute to research and development is high since AM is still developing and acceptance by industry has been surging in recent years. One of the key issues is the correlation of production parameters and specific alloy systems with the structure and properties of AM parts. A current challenge is the operando X-ray tomographic analysis of LPBF.

3.5.1. Cellular Structure

Thomson et al. and Du Plessis et al. have recently presented comprehensive reviews on the use of X-ray tomography in research related to additive manufacturing of metals with a focus on the effects of defects on mechanical properties.^[248,249] Del Guercio et al. reviewed the correlation between microstructure and mechanical performance of TiAl6V4 lattice structures.^[250] Amani et al. studied the compression behaviour of such lattice structures with X-ray tomography and finite element approaches.^[251] Some other works address the influence of defects such as pores and cracks induced e.g., by fatigue in TiAl6V4 alloys produced by metal LPBF.^[111,131] Furthermore, tomograms were even used as an input for numerical simulations.^[252] The structure of metallic parts produced by other processes such electron beam melting^[250] or extruded metal ink^[253,254] have been studied as well.

The interior of many additively manufactured metal parts is not as dense as conventional materials and tends to be porous. This can be due to limitations of the process or intentional, in

which case an almost cellular structure saves material and reduces weight. Regular lattices are common due to their predictable properties and therefore, the performance of cellular lattices is of interest. Pasini et al. studied regular octet and rhombicuboctahedron units deliberately fabricated with geometric imperfections.^[255] AlSi10Mg alloy was processed by LPBF, after which in-situ tomography was carried out in various states of uniaxial compression. The resulting data was compared to finite element simulations. It was found that the compressive response of the studied lattices differed from the simulations of the ideal structure, and this could be traced back to the imperfections of the lattice. An example from this work is presented in **Figure 16**.

3.5.2. Laser Powder Bed Fusion (LPBF)

Due to recent advances in X-ray imaging powder melting and sintering can be studied in situ and operando with very short time resolutions.^[256] This enables one to elucidate phenomena that occur during melting and rapid solidification during additive manufacturing, where, for example through LPBF, a laser beam selectively melts a part of a two-dimensional powder bed thus forming a continuous part layer by layer. Such experiments have already been carried out using X-ray radiography^[257,258] and/or diffraction.^[256,257,259] Recently, Parab et al. applied X-ray radiography to study laser-based additive manufacturing of metals,^[260] Guo et al. observed the dynamics of melt flow,^[261] and Chen et al. the keyhole in detail.^[262]

Parts printed with LPBF usually contain many pores similar to cast components. This severely limits their application potential although porosity has already being reduced down to 0.5% in some cases in the past 15 years.^[263] X-ray tomography allows one to analyse pore formation in detail and time-resolved. Tomography has various advantages over radiography including that edge effects of thin samples can be avoided and image superposition that is typical for radiography is no longer an issue.^[264] X-ray tomography can also help in improving production parameters and developing dedicated alloys for additive manufacturing.

A proof-of-concept operando tomographic experiment of the LPBF was conducted by the present authors for the first time. Pure aluminum powder was used as a model system to verify that

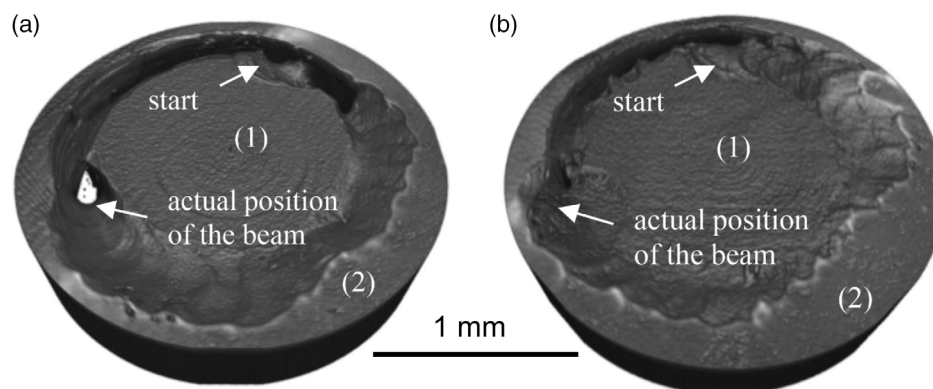


Figure 15. Rendered tomogram of a circular weld seam between a wrought aluminum alloy pin 1) and a die-cast aluminum alloy ring 2) as extracted from a tomography experiment taken at 100 tps with a) a static laser beam giving rise to pronounced weld arching and metal ejections and b) a beam oscillating 0.1 mm at 4 kHz, which produced a homogeneous weld seam. See also supplementary Video S1 and S2, Supporting Information. Reproduced with permission.^[233] Copyright 2021, Laser Institute of America.

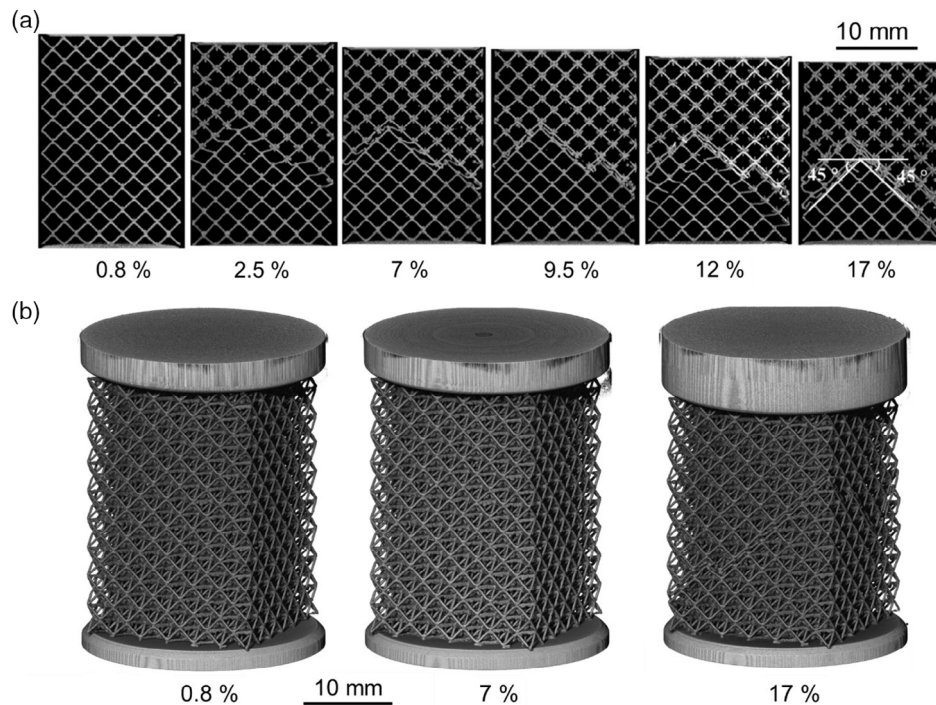


Figure 16. a) In-situ tomographic slices of a series of compression stages of a regular octet lattice structure produced by selective laser melting of AlSi10Mg alloy powder depicting successive failure. b) 3D-rendered tomograms at 3 of the stages in (a).^[255] Part a) reproduced with the permission from Elsevier.

loose powders can be processed even at the high rotation frequencies of the stage and that time resolution can be pushed to a limit that allows one to distinguish sample details without too much blurring. For this type of experiment, a similar setup and configuration was used as for laser welding.^[233] Pure aluminum powder was placed inside a cylindrical boron nitride crucible, which is largely transparent to X-rays and does not react with liquid aluminum. A laser pulse melted a rotating bed of aluminum powder and tomography was applied at a rate of 100 tps to resolve the sintering of the metallic powder under realistic production conditions. The temporal evolution of the aluminum powder particles during formation of the first molten layer during a simulated LPBF sintering was recorded along two complete circles of 2 mm diameter in 0.72 s at an effective beam speed of 17 mm s^{-1} .

The first circle completed after 0.36 s is shown in **Figure 17a,b**. Selected tomographic slices of the powder surface in **Figure 17a** as well as three-dimensionally rendered tomograms in **Figure 17b** at different times demonstrate the progression of the sintering. Individual melt lumps shown in different colours form at the position of the laser spot as the particles are melted by the laser beam. This effect is known as balling and usually appears at too low melting temperatures, i.e., too low laser beam energies, leading to melt pool instabilities and increasing at the same time the surface roughness.^[265] The lumps formed have an equivalent diameter of 0.2–0.5 mm and have been rounded off to approximately spherical due to surface tension. At the same time, the apparent density of the powder around the formed lumps decreases reflected by dark empty areas around the lumps in the tomoscopic slices shown in **Figure 17a**, which are also known

as denudation zones.^[266,267] The reason for this behaviour is the difference between the density of the molten aluminum and the apparent density of the powder bed. Furthermore, if the laser beam hits a powder region with low apparent density, as it can be observed in **Figure 17a** after 0.2 s, the resulting denudation zone around the following molten lumps increases in size as visible after 0.36 s. This underlines the importance to prepare a homogeneous power distribution layer by layer. The lumps remain separated from each other and essentially retain their original shape throughout the process until they solidify, as shown in **Figure 17b**. Furthermore, the stabilizing effect of a thin oxide layer on the reactive aluminum melt around the melt lumps, formed despite the surrounding technical nitrogen atmosphere, can also play a role.

The evolution of the total volume of molten powder as well as the porosity formed within the particles in the first circle is quantified in **Figure 18a**. The total volume of the molten powder increases almost linearly with time at a rate of $1.4 \text{ mm}^3 \text{ s}^{-1}$ up to 0.5 mm^3 after 0.36 s. **Figure 18a** also shows the porosity evolution as the total pore volume inside the lumps in the same period of time. After 0.18 s, the first pores appear, but quickly disappear again, indicating that all the material is still molten. The majority of the pores do not form until the first lumps begin to solidify after $\approx 0.28 \text{ s}$, resulting in a pore volume of $\approx 0.5 \times 10^{-3} \text{ mm}^3$, i.e., a porosity of 0.1% at 0.36 s after the laser beam has passed through the full circle, see **Figure 18a**.

The rapid solidification of molten regions is a characteristic of LPBF. In our experiment, the molten lumps solidify between 0.20 and 0.35 s after the beam has passed them depending on

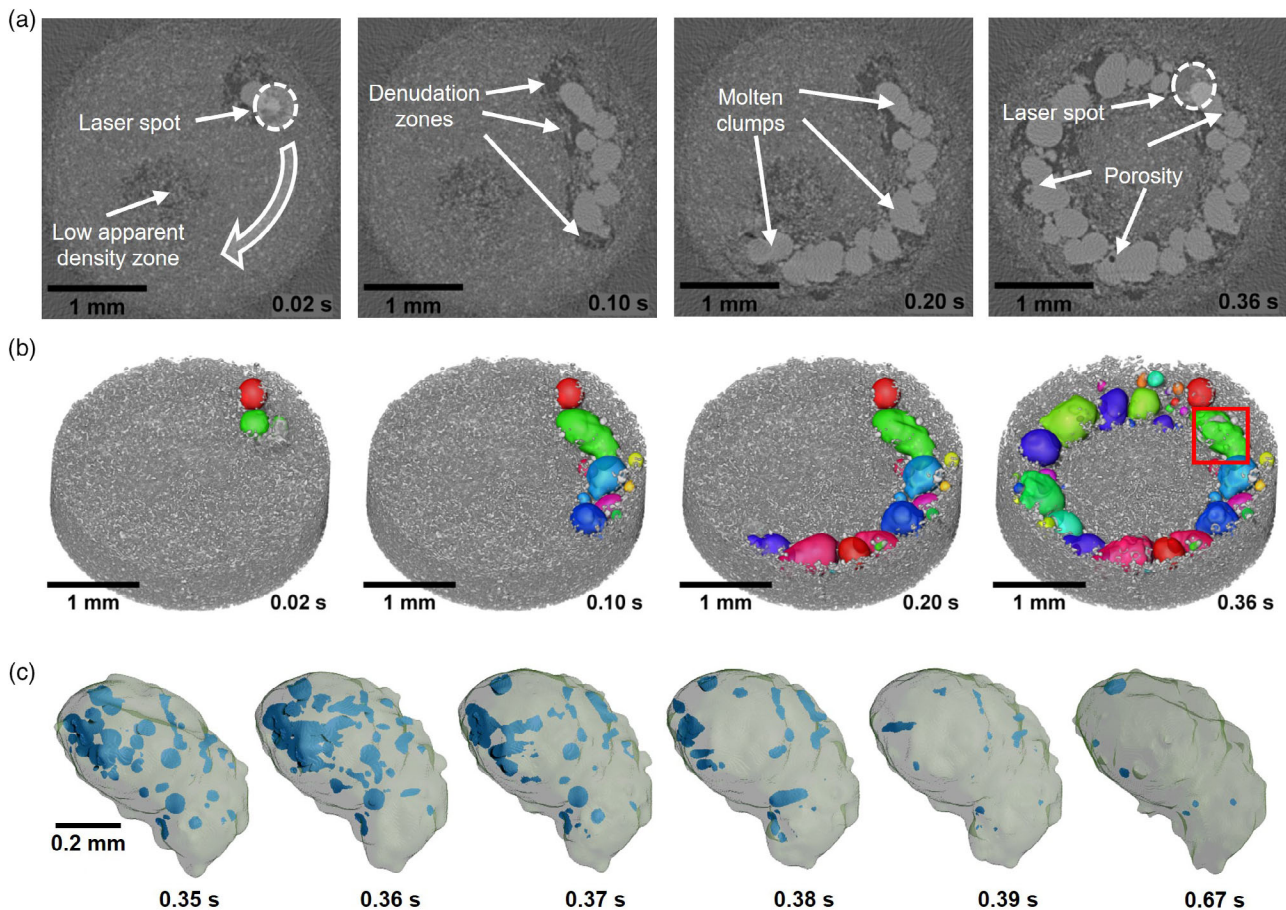


Figure 17. Evolution of pure aluminum powder during melting of the first layer of a powder bed by LPBF during the first 0.36 s. a) Selected tomographic slices of the progress of powder sintering and, b) the corresponding 3D-rendered tomograms showing sintered metal lumps. Different colours indicate separate aluminum lumps. c) Selected lump corresponding to the green lump marked by a red square in (b) showing the temporal evolution of porosity within (in cyan) from 0.35 to 0.39 s in steps of 10 ms, and at 0.67 s. The second remelting starts at 0.36 s and the lump is again solid at 0.67 s. See also Video S3 and S4, Supporting Information.

their size. Solidification is accompanied by the formation of porosity in the lumps since all residual gases cannot diffuse out fast enough to avoid being trapped.^[266,268–270] Figure 17c shows a selected lump corresponding to the green lump marked by a red square in Figure 17b. It shows the evolution of its porosity between 0.35 and 0.39 s in 10 ms steps. Between 0.35 and 0.36 s porosity increases in the course of solidification but decreases rapidly again between 0.36 and 0.39 s due to remelting of the material in the course of the second interaction with the laser beam. After 0.67 s, the lump solidifies a second time but with a notably reduced porosity of 0.25% compared to the original porosity of 4% as shown in Figure 18b, which underlines the advantages of a remelting step.^[271]

3.6. Industrial Tomography

In addition to its important role in research and development, a systematic application of X-ray tomography in industrial environments has become visible in recent years.^[27] Applications range from prototype development to the analysis of damage, failure, defects in parts to quality control. Under certain

circumstances, e.g., if testing is performed in seconds without having to take parts out of the production line and the analysis is carried out automatically, tomography can be used at lower costs than destructive or other means of manual testing. X-ray tomography as an NDT method is becoming increasingly popular, although it has to compete with more simple and faster methods such as X-ray radiography, laminography or ptychography.^[272] For this reason, temporal resolution is of great importance, because, as it is well known, time is money.

3.6.1. Prototypes

Many prototypes and new components require extensive evaluation before they can be manufactured in a pre-series. In many cases, closed-loop iteration is required to optimise parts step by step. This process is computerised and requires a bidirectional transfer of information between software and hardware. The production of metal parts and moulds based on Computer Aided Design (CAD) is currently predominant. The corresponding production step, from design to workpiece, is often carried out with Computerised Numerical Control (CNC) machines.

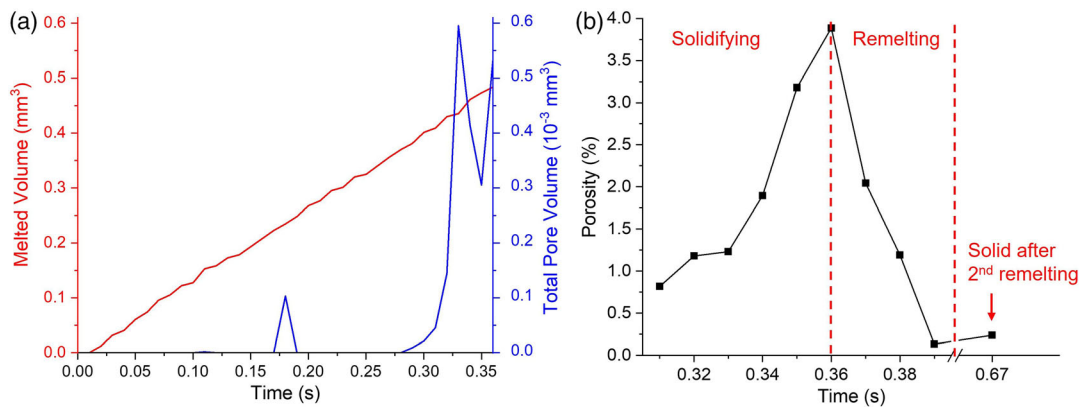


Figure 18. a) Temporal evolution of the total volume of melted powder (red curve) and the total pore volume inside the lumps (blue curve). b) Porosity evolution inside the single lump shown in Figure 17c during solidification between 0.31 and 0.36 s, remelting between 0.36 and 0.39 s by a second interaction with the laser beam and at the solid state after the second remelting.

In the reverse step, the digitisation of the prototype, tomography unfolds its full potential because, unlike visual devices such as laser scanners, it is able to transfer all real dimensions, contours and components, including those hidden inside the workpiece, to the computer. A prominent example are tools produced by additive manufacturing for medical applications.^[273,274] In addition, tomographic analysis can be an essential part of the quality assessment of components, supplier documentation or the initial sample inspection report for the approval of workpieces.

3.6.2. Damage Analysis, Defect Parts and Failure

Another very important topic in industrial development is the analysis of damage, defective parts and failures. This step is necessary to prevent parts from failing, which could damage the company's reputation, and to improve their performance. Real-time analysis under operating conditions or without destroying parts is only possible with NDT such as X-ray tomography, which allows for a high-precision visualisation of three-dimensional volumes and the analysis of hidden parts. The analysis of defects and failure in additive manufactured parts is an actual example where tomography is applied.^[249,275] The resulting digital archives are very important for a complete documentation also before possible further destructive analyses.

3.6.3. Reverse Engineering

Reverse engineering is the process carried out with the aim of obtaining information or a design from a product, in order to determine what its components are, how they interact with each other and what the manufacturing process might have been. It is regularly applied by many companies, e.g., to detect possible infringements of intellectual property rights.

X-ray tomography makes it possible to obtain a full three-dimensional digital twin of a sample and to extract information that can be directly imported into a computer to create a similar product or to analyse its properties with appropriate software in a typical reverse engineering procedure.^[276] As an example, Bauer et al. described the step-by-step process workflow for the case study of a turbine blade.^[31]

3.6.4. Quality Control and NDT

The main function of quality control in industry is to ensure that products or services meet minimum quality requirements. The process involves the collection and analysis of large amounts of data to ensure that production meets the specifications set by product engineers. If a product does not meet the minimum specifications or has some defective qualities, it is necessary to correct possible manufacturing deficiencies. This potentially avoids added costs and material waste. Typical defects in metal parts are dimensional deviations, wall thickness variations, casting defects, pores, blow holes, volume defects, inclusions, metal particles or agglomerates, initial cracks or even mechanical overstress during production. Whenever metallic parts are produced in combination with other materials, joint defects such as weld seams or insufficient adhesive bonding may occur.

To control the quality of a product, inspections or sample tests are carried out to verify that the product characteristics are optimal. Standard quality control procedures, in which a certain percentage of products is selected and removed from the production line from time to time, are time-consuming and costly. NDT quality control procedures such as X-ray radiography are more appropriate and faster. Although radiography is faster than tomography, the latter can provide three-dimensional information that may be beneficial and is gaining importance because the temporal resolution of commercial laboratory scanners has increased in recent years to a few seconds per tomogram.^[50] A trendsetting example is the latest generation of X-ray tomographic airport scanners, used for security rather than quality control, with throughput speeds of up to 0.5 m s^{-1} .^[84]

3.7. Batteries

Often it is not the properties of a metal that are of primary interest, but its behaviour in a complex system or operating device. A good example is a current research topic: the operando investigation of battery cells. Here, electrodes experience a large volume change when ions are incorporated or released during charge or discharge. Lithium-ion systems in particular are currently in the focus of research.^[277]

The time scales involved in battery cycling range from hours to days, thus enabling operando analyses where a battery is continuously (dis)charged and tomograms are obtained in regular intervals. Ebner et al. studied the electrochemical and mechanical degradation in lithium-ion batteries in this way almost a decade ago.^[278] An important point to consider is the reduction of radiation damage or impact on such sensitive electrochemical systems. Radiation-induced degradation of the electrolytes or local temperature gradients caused by a different absorption of radiation by the components must be kept low as batteries are very sensitive to this.^[279]

Research is mostly focused on improving existing commercial lithium-ion systems, but current demand for portable electronic devices and electromobility requires new anode and cathode materials.^[277] New systems are expected to offer higher potential capacity and be more cost-effective than current systems. One of the main problems is to ensure cycling stability to avoid degradation of the electrodes caused by extreme volume changes during cycling and to understand the function of specially designed electrolytes. Pietsch et al. have recently reviewed the possibilities of X-ray tomography for the examination of battery systems.^[280] Seitzman et al. studied the response of lithium to the solid-state electrolyte in an operando configuration^[281] and Le Houx et al. reviewed the possibilities of X-ray tomography for the characterisation of lithium-ion batteries.^[282]

Other promising systems such as lithium-sulphur pouch cells have recently been studied by laboratory X-ray tomography.^[283] Wang analysed sodium-ion batteries and the influence of tin particles by in situ hard X-ray nanotomography.^[284] Vanpeene et al. characterized the degradation of silicon-based anodes for lithium-ion batteries.^[285] Wilke et al. revealed the degradation mechanisms in lamellar iron foams during redox cycling at 800 °C for iron-air batteries.^[286] Over the past two years, intensive research has been carried out on solid-state electrodes for lithium batteries.^[281,287,288]

Some research focused on multi-scale or multi-method approaches.^[289] For example, Shearing et al. have conducted a comprehensive multi-length scale investigation of commercially available lithium-ion battery electrodes.^[290] Other scientists combined simultaneous electrochemical state measurements with X-ray diffraction and tomography to investigate batteries operando. These multi-method approaches help in correlating the state of charge with the evolution of the phases involved and the microstructure. Sun et al. visualized the morphological and compositional evolution in a solid-state lithium-sulphur cell operando with X-ray tomography and energy dispersive diffraction simultaneously^[291] as well as Elia et al. in aluminum-graphite batteries.^[292]

A greater challenge in the tomographic analysis of battery systems is the investigation of processes much faster than cycling as for example during cell failure. Yokoshima et al. applied fast X-ray radiography for an operando analysis of thermal runaway in lithium-ion batteries during penetration by a nail^[293] while Patel et al. investigated the thermal runaway of a lithium-ion battery combining accelerating rate calorimetry and multi-length scale ex-situ laboratory X-ray tomography.^[294] For the analysis of lithium-ion battery case ruptures Kong et al.

applied ex situ X-ray tomography.^[295] Finegan et al. studied thermal runaway of lithium-ion batteries with radiography and a temporal resolution of over 20 kfps.^[296] and ex situ with tomography.^[297,298]

At this point it is clear that X-ray tomography has to step forward to analyse fast phenomena in battery research. Yang et al. studied the motion of evolving particles in the drying process of battery electrodes dynamically with X-ray tomography at a rate of one tomogram each 30 s.^[299] Finegan et al. applied X-ray tomography at a rate of slightly more than 1 tps to study thermal runaway, but this was obviously still insufficient to elucidate the dynamic of the process in detail.^[300]

In a feasibility study, the present authors recently observed thermal runaway of a commercial alkaline AAAA battery at a tomographic acquisition rate of 10 tps, see **Figure 19**. Thermal runaway was induced by exposing the battery to an environment at ≈ 200 °C, which then led to a reaction of the battery constituents (see Figure 19b after 5 s), followed by the opening of the venting valve to release gas and lower the internal pressure (see Figure 19c after 7 s) and terminating with the full decomposition of the cell interior, better observed in the Video S5, Supporting Information.

4. Conclusions, New Developments and Future Trends

In the coming years, X-ray tomography and especially tomography will face new challenges in all areas of research, especially in materials science. Now that the methods have been established, further steps forward can be expected. This mission is only feasible through coordinated hardware and software developments and more powerful computing infrastructure such as GPU hardware, which goes hand in hand with more efficient algorithms to increase overall performance. The direction of development of tomography and tomography is set by future trends in research, but of course is limited by the technical possibilities.

Current and future trends point at more operando analyses of dynamic processes.^[88] Research interests are driving the addition of process-specific to traditional more material-specific analyses. Moreover, multi-method and multi-analyses are becoming increasingly important. In the field of materials research, materials in batteries or lightweight materials such as aluminum alloys on the one hand and metal production processes such as additive manufacturing on the other are gaining interest. In an industrial environment, the use of laboratory-based X-ray tomography systems for quality control or reverse engineering is becoming more popular and accessible thanks to recent improvements and automated data analysis. Finally, tomography offers the possibility to create a digital twin, i.e., an electronic version of a sample that allows for further virtual analysis, for example, the study of mechanical deformation as part of a finite element simulation analysis.

The combination of multi-method approaches with simultaneous in-situ measurements makes the integration of all requirements in a single experiment a major challenge.^[216] In this case, specific and properly designed sample environments will play an even more important role.

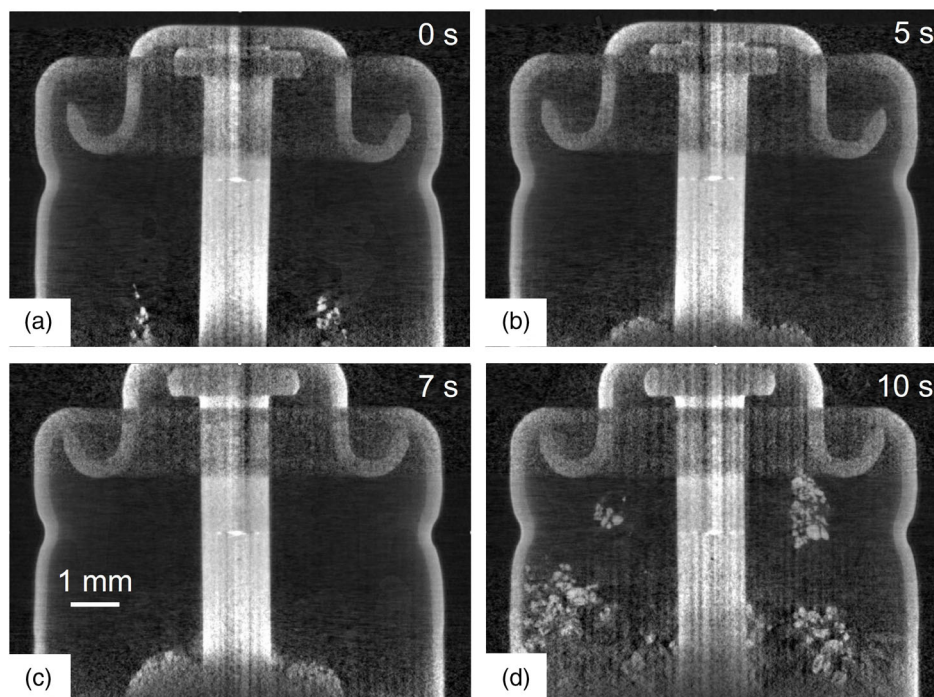


Figure 19. Slices from an X-ray tomoscopic measurement of the thermal runaway of a commercial alkaline AAAA battery exposed to external temperature of $\approx 200^\circ\text{C}$ after, a) 0 s, b) 5 s, c) 7 s, d) 10 s. Tomoscopy rate was 10 tps. See also Video S5, Supporting Information.

4.1. Hardware Developments

The development of high-brilliance and high-intensity 3rd generation synchrotron sources has brought X-ray tomography to its current state.^[3] Further hardware developments such as 4th generation synchrotrons, which produce an even brighter and more coherent photon beam, could expand the possibilities and push science to new limits.^[301] Similarly, micro- and nano-focus laboratory sources have been improving over the years. For example, novel liquid metal X-ray sources can achieve much higher intensities at certain energies compared to standard sources with solid targets, thanks to a liquid target and the associated higher output flux. Acquisition speeds of one tomogram per second have recently been reported.^[302]

Dedicated optics with special coatings and the continuous development of the speed and sensitivity of the cameras and indirect detectors also play their part.^[303] An example are the next-generation photon counting or direct converting detectors developed by the Medipix collaboration,^[304] which are more efficient and more than one order of magnitude faster than conventional indirect converting flat panel detectors.

In recent years, multi-beam methods have been developed for high-intensity X-ray sources such as synchrotron sources and free-electron lasers. Villanueva-Pérez demonstrated the possibility of splitting the main beam with a face-centred cubic splitter crystal (Si 001) into 8 reflections, which can later be recombined and focused on the sample and recorded, together with the main beam, to 9 individual projections with a single shot.^[305] Shirasawa et al. placed eight silicon single crystals in a parabolic configuration in front of the main beam, focused their main

reflection onto a sample and recorded the 9 projections in a similar manner.^[306] The same group also proposed an alternative solution using optical fibres to guide beams to a single camera.^[307] Voegeli et al. used a similar concept using a curved crystal with discrete silicon lamellae, but producing up to 18 diffracted beams.^[308] These approaches are restricted to a limited angle of incidence, which could be improved up to $\pm 70^\circ$ by combining different crystals in series, but at the expense of beam intensity.^[308] These are currently feasibility studies, but promise to improve imaging speed by orders of magnitude once the technology has become more mature. Since samples do not need to be rotated, further possibilities for more complicated sample environments are conceivable with such configurations. Rapid rotation of liquids or soft samples is neither possible nor recommended to avoid disturbing the sample. Tomography without rotation of the sample will allow for tomographic studies without the disturbance of radial g-forces at high acquisition rates.

Fast, laboratory-based tomography scanners can circumvent the limitations of synchrotron availability in certain cases. Under laboratory conditions, beam splitting is not an option as the flux of laboratory sources is many orders of magnitude lower compared to synchrotrons. However, there are other options for multi-beam configurations, such as using multiple sources and detectors to illuminate a sample simultaneously from many directions, where each source-detector pair takes a single projection and detectors are evenly distributed over an entire circle. The main disadvantage of this brute-force approach, apart from cost, is the limited number of projections, constrained by the geometric configuration of the source-detector pairs.

This could be solved in combination with recent software developments through which artificially intelligent algorithms are able to reconstruct 3D volumes from a reduced number of projections.^[309] Combining a multi-beam concept with a standard rotation stage could reduce the rotation angle from typically 360° in standard cone beam laboratory setups to $360^\circ n^{-1}$, where n is the number of source-detector pairs, and multiply the number of projections if necessary.

In an industrial environment where a product is normally transported on a conveyor belt and cannot be rotated accurately, a fast and non-rotating tomography configuration with automated and intelligent software analysis could enable quality control of every product and change the way quality control is currently done.

4.2. Software Developments

In the past decade, image analysis has improved considerably.^[310] Image processing has made a great leap in development thanks to methods of data science and artificial intelligence.^[311] The most significant advances include tomographic reconstruction and quantitative volume analyses.

More advanced methods such as interlaced reconstruction,^[86–88] incremental reconstruction^[2] or artificial intelligence supported methods^[89] will gain popularity. New reconstruction methods can further reduce the number of projections and therefore scan times, provide good reconstructions based on a reduced number of projections. Improvement in reconstruction time can pave the road towards real-time reconstruction algorithms.^[86,312–314] This will allow a scientist to react to tomographic measurements and, e.g., change a processing parameter of an experiment in real time. Most of the new algorithms apply artificial intelligence to improve reconstruction. Pelt et al. improved tomographic reconstruction from limited data by employing convolutional neural networks,^[309] Hendriksen applied deep learning and denoising steps to improve image resolution.^[315] Zhang et al. reviewed all the methods recently.^[89]

For the quantification of tomographic 3D volumetric data, advanced feature segmentation and recognition analysis algorithms are required.^[316,317] For this purpose, digital volume correlation^[318–320] and particle tracking methods have been developed in the past decade.^[321,322] Nevertheless, the actual trend focuses on machine learning tools. Strohmman et al. used a convolutional neural network for the segmentation of phases in AlSi alloys.^[323] Hendriksen et al. applied machine learning for improving image resolution to X-ray tomography measurements^[324] and deep denoising without high-quality reference data.^[92]

In conclusion, at the current pace, X-ray tomography will bring many more innovations to researchers in the near future and, concurrently, more areas of materials science and processing will apply the then available methods.

Supporting Information

Supporting Information is available from the Wiley Online Library or from the author.

Acknowledgements

The Deutsche Forschungsgemeinschaft funded the work through Reinhart-Koselleck project number 408321454, Ba 1170/40 and the German Bundesministerium für Bildung und Forschung through project 05K18KTA. We acknowledge the Paul Scherrer Institut, Villigen, Switzerland for providing synchrotron radiation beam time at the TOMCAT beamline X02DA of the SLS, and we would like to thank in particular Dr. Ch. Schlepütz who helped during the synchrotron measurements. We thank N. von der Eltz, Dr. D. Dittrich and Dr. S. Börner for support during the operando additive manufacturing experiments and Dr. O. Andersen for providing the Al-Si fibres.

Open Access funding enabled and organized by Projekt DEAL.

Conflict of Interest

The authors declare no conflict of interest.

Keywords

imaging, metals, time-resolved, tomography, tomography, X-ray

Received: September 16, 2022

Revised: November 28, 2022

Published online:

- [1] R. Hanke, T. Fuchs, N. Uhlmann, *Nucl. Instrum. Methods Phys. Res., Sect. A* **2008**, 591, 14.
- [2] F. García-Moreno, P. H. Kamm, T. R. Neu, F. Bülk, R. Mokso, C. M. Schlepütz, M. Stampanoni, J. Banhart, *Nat. Commun.* **2019**, 10, 3762.
- [3] F. García-Moreno, P. H. Kamm, T. R. Neu, F. Bülk, M. A. Noack, M. Wegener, N. von der Eltz, C. M. Schlepütz, M. Stampanoni, J. Banhart, *Adv. Mater.* **2021**, 33, 2104659.
- [4] E. Maire, P. J. Withers, *Int. Mater. Rev.* **2014**, 59, 1.
- [5] J. Banhart, *Advanced Tomographic Methods in Materials Research and Engineering*, Oxford University Press, Oxford **2008**.
- [6] L. Holzer, M. Cantoni, in *Nanofabrication Using Focused Ion and Electron Beams: Principles and Applications* (Eds: I. Utke, S. Moshkalev, P. Russell), Oxford University Press, New York, NY **2012**, p. 410.
- [7] M. W. Phaneuf, in *Introduction to Focused Ion Beams: Instrumentation, Theory, Techniques and Practice* (Eds: L. A. Giannuzzi, F. A. Stevie), Springer US, Boston, MA **2005**, p. 143.
- [8] T. F. Kelly, M. K. Miller, *Rev. Sci. Instrum.* **2007**, 78, 031101.
- [9] B. Gault, A. Chiaramonti, O. Cojocaru-Mirédin, P. Stender, R. Dubosq, C. Freysoldt, S. K. Mäkinen, T. Li, M. Moody, J. M. Cairney, *Nat. Rev. Methods Primers* **2021**, 1, 51.
- [10] A. Cerezo, P. H. Clifton, S. Lozano-Perez, P. Panayi, G. Sha, G. D. W. Smith, *Microsc. Microanal.* **2007**, 13, 408.
- [11] N. Kardjilov, I. Manke, A. Hilger, M. Strobl, J. Banhart, *Mater. Today* **2011**, 14, 248.
- [12] M. T. M. Khairi, S. Ibrahim, M. A. M. Yunus, M. Faramarzi, G. P. Sean, J. Puspanathan, A. Abid, *Measurement* **2019**, 146, 490.
- [13] T. Dyakowski, L. F. C. Jeanmeure, A. J. Jaworski, *Powder Technol.* **2000**, 112, 174.
- [14] M. Kawasaki, *Optical Coherence Tomography*, InTech, Rijeka, Croatia **2013**.
- [15] S. Koneti, L. Roiban, F. Dalmas, C. Langlois, A.-S. Gay, A. Cabiac, T. Grenier, H. Banjak, V. Maxim, T. Epicier, *Mater. Charact.* **2019**, 151, 480.

- [16] D. L. Bailey, D. W. Townsend, P. E. Valk, M. N. Maisey, *Positron Emission Tomography*, Springer, London **2005**.
- [17] P. J. Withers, C. Bouman, S. Carmignato, V. Cnudde, D. Grimaldi, C. K. Hagen, E. Maire, M. Manley, A. Du Plessis, S. R. Stock, *Nat. Rev. Methods Primers* **2021**, 1, 18.
- [18] S. Gray, *Medical Tomography*, Foster Academics, New York **2018**.
- [19] T. Schwarz, J. Saunders, *Veterinary Computed Tomography*, Wiley, Oxford **2011**.
- [20] E. Bercovich, M. C. Javitt, *Rambam Maimonides Med. J.* **2018**, 9, e0034.
- [21] J. Baruchel, J.-Y. Buffière, E. Maire, P. Merie, G. Peix, *X-ray Tomography in Material Science*, Hermes Science Publications, Hermes, Paris **2000**.
- [22] E. Maire, J. Y. Buffière, L. Salvo, J. J. Blandin, W. Ludwig, J. M. Létang, *Adv. Eng. Mater.* **2001**, 3, 539.
- [23] R. Mizutani, Y. Suzuki, *Micron* **2012**, 43, 104.
- [24] V. Cnudde, M. N. Boone, *Earth-Sci. Rev.* **2013**, 123, 1.
- [25] S. Hughes, in *Computed Tomography - Special Applications* (Ed: D. L. Saba), InTech, Croatia **2011**, p. 57.
- [26] M. Bieberle, F. Barthel, *Chem. Eng. J.* **2016**, 285, 218.
- [27] L. De Chiffre, S. Carmignato, J. P. Kruth, R. Schmitt, A. Weckenmann, *CIRP Ann.* **2014**, 63, 655.
- [28] A. Hussain, S. Akhtar, *Arabian J. Sci. Eng.* **2017**, 42, 925.
- [29] J. Kastner, C. Heinzl, in *Integrated Imaging and Vision Techniques for Industrial Inspection: Advances and Applications* (Eds: Z. Liu, H. Ukida, P. Ramuhalli, K. Niel), Springer London, London **2015**, p. 227.
- [30] D. O. Thomson, D. E. Chimenti, *Review of Progress in Quantitative Nondestructive Evaluation*, Vol. 17A, Plenum Press, New York, NY **1998**.
- [31] F. Bauer, M. Schropp, J. Szijarto, *Precis. Eng.* **2019**, 60, 63.
- [32] F. Retraint, J. M. Dinten, R. Campagnolo, F. Peyrin, in *Review of Progress in Quantitative Nondestructive Evaluation*, Vol. 17A (Eds: D. O. Thompson, D. E. Chimenti), Springer US, Boston, MA **1998**, p. 363.
- [33] ASM, *Nondestructive Evaluation and Quality Control*, Vol. 17, ASM International, Washington **1992**.
- [34] G. N. Hounsfield, *Br. J. Radiol.* **1973**, 46, 1016.
- [35] D. P. Boyd, J. L. Couch, S. A. Napel, D. L. Parker, K. R. Peschmann, R. E. Rand, W. B. Herrmannsfeldt, presented at *Int. Workshop on Physics and Engineering in Medical Imaging*, SPIE, Pacific Grove **1982**.
- [36] A. J. Feiring, J. A. Rumberger, S. J. Reiter, D. J. Skorton, S. M. Collins, M. J. Lipton, C. B. Higgins, S. Ell, M. L. Marcus, *Circulation* **1985**, 72, 1355.
- [37] S. J. Reiter, J. A. Rumberger, A. J. Feiring, W. Stanford, M. L. Marcus, *Circulation* **1986**, 74, 890.
- [38] P. G. Lutran, K. M. Ng, E. P. Delikat, *Ind. Eng. Chem. Res.* **1991**, 30, 1270.
- [39] A. Kantzas, *AIChE J.* **1994**, 40, 1254.
- [40] K. Hori, K. Kawanishi, H. Hamamura, M. Ochi, M. Akai, presented at *The 4TH Int. Topical Meeting on Nuclear Thermal Hydraulics, Operations and Safety*, Taipei, Taiwan, April 1994.
- [41] M. Bieberle, U. Hampel, *Meas. Sci. Technol.* **2006**, 17, 2057.
- [42] M. Bieberle, F. Fischer, E. Schleicher, U. Hampel, D. Koch, K. S. D. C. Aktay, H.-J. Menz, H.-G. Mayer, *Appl. Phys. Lett.* **2007**, 91, 123516.
- [43] M. Neumann, M. Bieberle, M. Wagner, A. Bieberle, U. Hampel, *Meas. Sci. Technol.* **2019**, 30, 084001.
- [44] D. Paganin, S. C. Mayo, T. E. Gureyev, P. R. Miller, S. W. Wilkins, *J. Microsc.* **2002**, 206, 33.
- [45] R. Fitzgerald, *Phys. Today* **2000**, 53, 23.
- [46] T. A. Siewert, D. W. Fitting, D. A. Shepherd, M. W. Austin, C. N. McCowan, in *Review of Progress in Quantitative Nondestructive Evaluation* (Eds: D. O. Thompson, D. E. Chimenti), Springer US, Boston, MA **1990**, p. 383.
- [47] W. E. Cryslar, *Am. J. Roentgenol.* **1970**, 109, 619.
- [48] H. Sklebitz, J. Haendle, *Am. J. Roentgenol.* **1983**, 140, 1247.
- [49] A. Vamvakeros, S. D. M. Jacques, M. Di Michiel, D. Matras, V. Middelkoop, I. Z. Ismagilov, E. V. Matus, V. V. Kuznetsov, J. Drnec, P. Senecal, A. M. Beale, *Nat. Commun.* **2018**, 9, 4751.
- [50] J. Dewanckele, B. Marijn, C. Frederik, L. Denisvan, M. Arnop, *J. Microsc.* **2020**, 277, 197.
- [51] D. Vavrik, J. Jakubek, I. Kumpova, M. Pichotka, *J. Instrum.* **2017**, 12, C02010.
- [52] P. H. Kamm, F. Garcia-Moreno, C. M. Schlepueetz, <http://resolution.tomoscopia.net> (accessed: August 2022).
- [53] M. P. Olbinado, V. Cantelli, O. Mathon, S. Pascarelli, J. Grenzer, A. Pelka, M. Roedel, I. Prencipe, A. L. Garcia, U. Helbig, D. Kraus, U. Schramm, T. Cowan, M. Scheel, P. Pradel, T. D. Resseguier, A. Rack, *J. Phys. D: Appl. Phys.* **2018**, 51, 055601.
- [54] C. Behrens, F. J. Decker, Y. Ding, V. A. Dolgashev, J. Frisch, Z. Huang, P. Krejčík, H. Loos, A. Lutman, T. J. Maxwell, J. Turner, J. Wang, M. H. Wang, J. Welch, J. Wu, *Nat. Commun.* **2014**, 5, 3762.
- [55] P. Vagovič, T. Sato, L. Mikeš, G. Mills, R. Graceffa, F. Mattsson, P. Villanueva-Perez, A. Ershov, T. Faragó, J. Uličný, H. Kirkwood, R. Letrun, R. Mokso, M.-C. Zdora, M. P. Olbinado, A. Rack, T. Baumbach, J. Schulz, A. Meents, H. N. Chapman, A. P. Mancuso, *Optica* **2019**, 6, 1106.
- [56] W. Ludwig, M. Herbig, J. Y. Buffière, P. Reischig, A. King, H. Proudhon, presented at *Mecatmat 2010 - Nouvelles approches en mécanique des matériaux*, Aussois, France, January 2010.
- [57] H. Poulsen, *J. Appl. Crystallogr.* **2012**, 45, 1084.
- [58] D. Juul Jensen, H. F. Poulsen, Å. Kvik, in *Encyclopedia of Materials: Science and Technology* (Eds: K. H. J. Buschow, R. W. Cahn, M. C. Flemings, B. Ilschner, E. J. Kramer, S. Mahajan, P. Veysière), Elsevier, Oxford **2005**, p. 1.
- [59] J. J. Rehr, A. L. Ankudinov, *Coord. Chem. Rev.* **2005**, 249, 131.
- [60] F. Garcia-Moreno, P. H. Kamm, T. R. Neu, J. Banhart, *J. Synchrotron Radiat.* **2018**, 25, 1505.
- [61] S. Sanchez, V. Fernandez, S. E. Pierce, P. Tafforeau, *Nat. Protoc.* **2013**, 8, 1708.
- [62] V. Van Nieuwenhove, J. De Beenhouwer, F. De Carlo, L. Mancini, F. Marone, J. Sijbers, *Opt. Express* **2015**, 23, 27975.
- [63] M. Boin, A. Haibel, *Opt. Express* **2006**, 14, 12071.
- [64] B. Münch, P. Trtik, F. Marone, M. Stampanoni, *Opt. Express* **2009**, 17, 8567.
- [65] G. R. Davis, J. C. Elliott, *Nucl. Instrum. Methods Phys. Res., Sect. A* **1997**, 394, 157.
- [66] R. A. Brooks, G. D. Chiro, *Phys. Med. Biol.* **1976**, 21, 390.
- [67] G. T. Herman, *Phys. Med. Biol.* **1979**, 24, 81.
- [68] A. Mouton, N. Megherbi, K. Van Slambrouck, J. Nuyts, T. P. Breckon, *J. Xray Sci. Technol.* **2013**, 21, 193.
- [69] L. M. Lohse, A.-L. Robisch, M. Topperwien, S. Maretzke, M. Krenkel, J. Hagemann, T. Salditt, *J. Synchrotron Radiat.* **2020**, 27, 852.
- [70] T. Weitkamp, D. Haas, D. Wegrzynek, A. Rack, *J. Synchrotron Radiat.* **2011**, 18, 617.
- [71] R. Mokso, F. Marone, S. Irvine, M. Nyvlt, D. Schwyn, K. Mader, G. K. Taylor, H. G. Krapp, M. Skeren, M. Stampanoni, *J. Phys. D: Appl. Phys.* **2013**, 46, 494004.
- [72] M. Bührer, M. Stampanoni, X. Rochet, F. Buchi, J. Eller, F. Marone, *J. Synchrotron Radiat.* **2019**, 26, 1161.
- [73] P. J. Withers, *Mater. Today* **2007**, 10, 26.
- [74] S. Flenner, M. Storm, A. Kubec, E. Longo, F. Doring, D. M. Pelt, C. David, M. Muller, I. Greving, *J. Synchrotron Radiat.* **2020**, 27, 1339.
- [75] R. Kumar, J. Villanova, P. Lhuissier, L. Salvo, *Acta Mater.* **2019**, 166, 18.

- [76] E. Zschech, M. Löffler, P. Krüger, J. Gluch, K. Kutukova, I. Zgłobicka, J. Silomon, R. Rosenkranz, Y. Standke, E. Topal, *Pract. Metall.* **2018**, 55, 539.
- [77] R. Mokso, C. M. Schlepütz, G. Theidel, H. Billich, E. Schmid, T. Celcer, G. Mikuljan, L. Sala, F. Marone, N. Schlumpf, M. Stampanoni, *J. Synchrotron Radiat.* **2017**, 24, 1250.
- [78] D. A. Schwyn, R. Mokso, S. M. Walker, M. Doube, M. Wicklein, G. K. Taylor, M. Stampanoni, H. G. Krapp, *Synchrotron Radiat. News* **2013**, 26, 4.
- [79] S. M. Walker, D. A. Schwyn, R. Mokso, M. Wicklein, T. Müller, M. Doube, M. Stampanoni, H. G. Krapp, G. K. Taylor, *PLoS Biol.* **2014**, 12, e1001823.
- [80] J. H. Radon, *Ber. Verh. Sächs. Akad. Wiss. Leipzig* **1917**, 69, 262.
- [81] W. van Aarle, W. J. Palenstijn, J. Cant, E. Janssens, F. Bleichrodt, A. Dabravolski, J. De Beenhouwer, K. Joost Batenburg, J. Sijbers, *Opt. Express* **2016**, 24, 25129.
- [82] A. Biguri, M. Dosanjh, S. Hancock, M. Soleimani, *Biomed. Phys. Eng. Express* **2016**, 2, 055010.
- [83] D. Gursoy, F. De Carlo, X. Xiao, C. Jacobsen, *J. Synchrotron Radiat.* **2014**, 21, 1188.
- [84] Analogic, ConneCT, <https://www.analogic.com/imaging-and-detection/checkpoint/> (accessed: August 2022).
- [85] L. A. Feldkamp, L. C. Davis, J. W. Kress, *J. Opt. Soc. Am. A* **1984**, 1, 612.
- [86] K. A. Mohan, S. V. Venkatakrishnan, J. W. Gibbs, E. B. Gulsoy, X. Xiao, M. D. Graef, P. W. Voorhees, C. A. Bouman, *IEEE Trans. Comput. Imaging* **2015**, 1, 96.
- [87] B. M. Patterson, N. L. Cordes, K. Henderson, X. Xiao, N. Chawla, in *Materials Discovery and Design: By Means of Data Science and Optimal Learning* (Eds: T. Lookman, S. Eidenbenz, F. Alexander, C. Barnes), Springer International Publishing, Cham **2018**, p. 129.
- [88] A. J. Shahani, X. Xiao, E. M. Lauridsen, P. W. Voorhees, *Mater. Res. Lett.* **2020**, 8, 462.
- [89] Z. Zhang, E. Seeram, *J. Med. Imaging Radiat. Sci.* **2020**, 51, 671.
- [90] Z. Liu, T. Bicer, R. Kettimuthu, D. Gursoy, F. De Carlo, I. Foster, *J. Opt. Soc. Am. A* **2020**, 37, 422.
- [91] A. A. Hendriksen, D. M. Pelt, K. J. Batenburg, *Trans. Comput. Imaging* **2020**, 6, 1320.
- [92] A. A. Hendriksen, M. Bühner, L. Leone, M. Merlini, N. Vigano, D. M. Pelt, F. Marone, M. di Michiel, K. J. Batenburg, *Sci. Rep.* **2021**, 11, 11895.
- [93] J. Schindelin, I. Arganda-Carreras, E. Frise, V. Kaynig, M. Longair, T. Pietzsch, S. Preibisch, C. Rueden, S. Saalfeld, B. Schmid, J.-Y. Tinevez, D. J. White, V. Hartenstein, K. Eliceiri, P. Tomancak, A. Cardona, *Nat. Methods* **2012**, 9, 676.
- [94] S. Van der Walt, J. L. Schönberger, J. Nunez-Iglesias, F. Boulogne, J. D. Warner, N. Yager, E. Gouillart, T. Yu, *PeerJ* **2014**, 2, e453.
- [95] O. Stamati, E. Andò, E. Roubin, R. Cailletaud, M. Wiebicke, G. Pinzon, C. Couture, R. Hurley, C. R. Caulk, D. Caillerie, T. Matsushima, P. Besuelle, F. Bertoni, T. Arnaud, A. Ortega Laborin, R. Rorato, Y. Sun, A. Tengattini, O. Okubadejo, J.-B. Colliat, M. Saadatfar, F. Garcia, E. C. Papazoglou, I. Vego, S. Brisard, J. Dijkstra, G. Birmpilis, *J. Open Source Software* **2020**, 5, 2286.
- [96] A. Fedorov, R. Beichel, J. Kalpathy-Cramer, J. Finet, J.-C. Fillion-Robin, S. Pujol, C. Bauer, D. Jennings, F. Fennessy, M. Sonka, J. Buatti, S. Aylward, J. V. Miller, S. Pieper, R. Kikinis, *Magn. Reson. Imaging* **2012**, 30, 1323.
- [97] T. Farago, S. Gasilov, I. Emslie, M. Zuber, L. Helfen, M. Vogelgesang, T. Baumbach, *J. Synchrotron Radiat.* **2022**, 29, 916.
- [98] A. Rack, F. Garcia-Moreno, T. Baumbach, J. Banhart, *J. Synchrotron Radiat.* **2009**, 16, 432.
- [99] A. Rack, F. Garcia-Moreno, C. Schmitt, O. Betz, A. Cecilia, A. Ershov, T. Rack, J. Banhart, S. Zabler, *J. Xray Sci. Technol.* **2010**, 18, 429.
- [100] A. Rack, F. Garcia-Moreno, O. Betz, S. Zabler, C. Schmitt, T. D. Rolo, A. Ershov, T. Rack, L. Helfen, J. Banhart, T. Baumbach, in *2008 IEEE Nuclear Science Symp. Medical Imaging Conf. (2008 Nss/Mic)*, Vol. 1–9, IEEE, Piscataway, NJ **2009**, p. 5449.
- [101] J. Villanova, R. Daudin, P. Lhuissier, D. Jauffrès, S. Lou, C. L. Martin, S. Labouré, R. Tucoulou, G. Martínez-Criado, L. Salvo, *Mater. Today* **2017**, 20, 354.
- [102] W. Yashiro, W. Voegeli, H. Kudo, *Appl. Sci.* **2021**, 11, 8868.
- [103] Fast-Tomography, <http://tinyurl.com/Fast-Tomography> (accessed: June 2018).
- [104] A. Cecilia, A. Rack, P. A. Douissard, T. Martin, T. dos Santos Rolo, P. Vagovič, E. Hamann, T. van de Kamp, A. Riedel, M. Fiederle, T. Baumbach, *Nucl. Instrum. Methods Phys. Res., Sect. A* **2011**, 648, S321.
- [105] A. Momose, W. Yashiro, S. Harasse, H. Kuwabara, *Opt. Express* **2011**, 19, 8423.
- [106] H. Takano, M. Morikawa, S. Konishi, H. Azuma, S. Shimomura, Y. Tsusaka, S. Nakano, N. Kosaka, K. Yamamoto, Y. Kagoshima, *J. Phys. Conf. Ser.* **2013**, 463, 012025.
- [107] T. dos Santos Rolo, A. Ershov, T. van de Kamp, T. Baumbach, *Proc. Natl. Acad. Sci.* **2014**, 111, 3921.
- [108] R. Mokso, D. A. Schwyn, S. M. Walker, M. Doube, M. Wicklein, T. Müller, M. Stampanoni, G. K. Taylor, H. G. Krapp, *Sci. Rep.* **2015**, 5, 8727.
- [109] E. Maire, C. Le Bourlot, J. Adrien, A. Mortensen, R. Mokso, *Int. J. Fract.* **2016**, 200, 3.
- [110] M. F. Ashby, *Materials Selection in Mechanical Design*, Butterworth-Heinemann, Amsterdam **2016**.
- [111] R. Biswal, X. Zhang, M. Shamir, A. Al Mamun, M. Awd, F. Walther, A. Khadar Syed, *Addit. Manuf.* **2019**, 28, 517.
- [112] M. Saadatfar, M. Mukherjee, M. Madadi, G. E. Schröder-Turk, F. Garcia-Moreno, F. M. Schaller, S. Hutzler, A. P. Sheppard, J. Banhart, U. Ramamurty, *Acta Mater.* **2012**, 60, 3604.
- [113] Z. Li, N. Limodin, A. Tandjaoui, P. Quaegebeur, J.-F. Witz, D. Balloy, *Mater. Sci. Eng., A* **2020**, 794, 139920.
- [114] C. Puncreobutr, P. D. Lee, R. W. Hamilton, A. B. Phillion, *JOM* **2012**, 64, 89.
- [115] D. A. H. Hanaor, L. Hu, W. H. Kan, G. Proust, M. Foley, I. Karaman, M. Radovic, *Mater. Sci. Eng., A* **2016**, 672, 247.
- [116] J. J. Williams, K. E. Yazzie, E. Padilla, N. Chawla, X. Xiao, F. De Carlo, *Int. J. Fatigue* **2013**, 57, 79.
- [117] G. Xue, T. Nakamura, N. Fujimura, K. Takahashi, H. Oguma, A. Takeuchi, M. Uesugi, K. Uesugi, *Eng. Fract. Mech.* **2022**, 263, 108308.
- [118] A. Junet, A. Messenger, X. Boulnat, A. Weck, E. Boller, L. Helfen, J.-Y. Buffiere, *Scr. Mater.* **2019**, 171, 87.
- [119] M. Wicke, A. Brueckner-Foit, T. Kirsten, M. Zimmermann, F. Buelbuel, H. J. Christ, *Int. J. Fatigue* **2019**, 119, 102.
- [120] S. P. Knight, M. Salazar, A. R. Trueman, *Corros. Sci.* **2011**, 53, 727.
- [121] A. E. Paz y Puente, D. C. Dunand, *Intermetallics* **2018**, 101, 108.
- [122] O. Lame, D. Bellet, M. D. Michiel, D. Bouvard, *Nucl. Instrum. Methods Phys. Res., Sect. B* **2003**, 200, 287.
- [123] T. Seidel, M. Fink, T. Hutsch, O. Andersen, in *Proc. 11th Int. Conf. Porous Metals and Metallic*, Cham **2020**.
- [124] E. Maire, J. C. Grenier, L. Babout, *Mater. Sci. Forum* **2006**, 519–521, 821.
- [125] S. Karagadde, P. D. Lee, B. Cai, J. L. Fife, M. A. Azeem, K. M. Kareh, C. Puncreobutr, D. Tsivoulas, T. Connolley, R. C. Atwood, *Nat. Commun.* **2015**, 6, 8300.
- [126] C. Puncreobutr, P. D. Lee, R. W. Hamilton, B. Cai, T. Connolley, *Metall. Mater. Trans. A* **2013**, 44, 5389.
- [127] M. A. A. Khan, A. K. Sheikh, B. S. Al-Shaer, in *Evolution of Metal Casting Technologies: A Historical Perspective* (Eds: M. A. A. Khan,

- A. K. Sheikh, B. S. Al-Shaer), Springer International Publishing, Cham **2017**, p. 1.
- [128] J. Y. Buffière, S. Savelli, P. H. Jouneau, E. Maire, R. Fougères, *Mater. Sci. Eng., A* **2001**, *316*, 115.
- [129] I. Maskery, N. T. Aboulkhair, M. R. Corfield, C. Tuck, A. T. Clare, R. K. Leach, R. D. Wildman, I. A. Ashcroft, R. J. M. Hague, *Mater. Charact.* **2016**, *111*, 193.
- [130] S. Tammam-Williams, P. J. Withers, I. Todd, P. B. Prangnell, *Sci. Rep.* **2017**, *7*, 7308.
- [131] W. Liu, C. Chen, S. Shuai, R. Zhao, L. Liu, X. Wang, T. Hu, W. Xuan, C. Li, J. Yu, J. Wang, Z. Ren, *Mater. Sci. Eng., A* **2020**, *797*, 139981.
- [132] L. Babout, E. Maire, J. Y. Buffière, R. Fougères, *Acta Mater.* **2001**, *49*, 2055.
- [133] M. De Giovanni, J. M. Warnett, M. A. Williams, P. Srirangam, *J. Alloys Compd.* **2017**, *727*, 353.
- [134] M. Mukherjee, F. Garcia-Moreno, C. Jiménez, A. Rack, J. Banhart, *Acta Mater.* **2017**, *131*, 156.
- [135] Anonymous, *Modern Casting* **2021**, *111*, 26.
- [136] O. Ludwig, M. Dimichiel, L. Salvo, M. Suéry, P. Falus, *Metall. Mater. Trans. A* **2005**, *36*, 1515.
- [137] M. Suéry, S. Terzi, B. Mireux, L. Salvo, J. Adrien, E. Maire, *JOM* **2012**, *64*, 83.
- [138] L. Salvo, P. Lhuissier, M. Scheel, S. Terzi, M. Di Michiel, E. Boller, J. A. Taylor, A. K. Dahle, M. Suéry, *Trans. Indian Inst. Met.* **2012**, *65*, 623.
- [139] H. Nguyen-Thi, L. Salvo, R. H. Mathiesen, L. Arnberg, B. Billia, M. Suery, G. Reinhart, *C. R. Phys.* **2012**, *13*, 237.
- [140] L. Salvo, M. Di Michiel, M. Scheel, P. Lhuissier, B. Mireux, M. Suéry, *Mater. Sci. Forum* **2012**, *706–709*, 1713.
- [141] D. Tolnai, P. Townsend, G. Requena, L. Salvo, J. Lendvai, H. P. Degischer, *Acta Mater.* **2012**, *60*, 2568.
- [142] Q. Zhang, D. Sun, S. Pan, M. Zhu, *Int. J. Heat Mass Transfer* **2020**, *146*, 118838.
- [143] S. Terzi, J. A. Taylor, Y. H. Cho, L. Salvo, M. Suéry, E. Boller, A. K. Dahle, *Acta Mater.* **2010**, *58*, 5370.
- [144] J. M. Yu, N. Wanderka, A. Rack, R. Daudin, E. Boller, H. Markötter, A. Manzoni, F. Vogel, T. Arlt, I. Manke, J. Banhart, *Acta Mater.* **2017**, *129*, 194.
- [145] S. Terzi, L. Salvo, M. Suery, A. K. Dahle, E. Boller, *Acta Mater.* **2010**, *58*, 20.
- [146] N. Limodin, L. Salvo, E. Boller, M. Suéry, M. Felberbaum, S. Gaillière, K. Madi, *Acta Mater.* **2009**, *57*, 2300.
- [147] J. L. Fife, P. W. Voorhees, *Acta Mater.* **2009**, *57*, 2418.
- [148] M. Bedel, G. Reinhart, A. A. Bogno, C. A. Gandin, S. Jacomet, E. Boller, H. Nguyen-Thi, H. Henein, *Acta Mater.* **2015**, *89*, 234.
- [149] M. Y. Wang, J. J. Williams, L. Jiang, F. De Carlo, T. Jing, N. Chawla, *Scr. Mater.* **2011**, *65*, 855.
- [150] W. Kurz, M. Rappaz, R. Trivedi, *Int. Mater. Rev.* **2020**, *66*, 30.
- [151] B. Cai, J. Wang, A. Kao, K. Pericleous, A. Phillion, R. Atwood, P. Lee, *Acta Mater.* **2016**, *117*, 160.
- [152] N. Limodin, L. Salvo, M. Suéry, M. DiMichiel, *Acta Mater.* **2007**, *55*, 3177.
- [153] J. L. Fife, J. W. Gibbs, E. B. Gulsoy, C. L. Park, K. Thornton, P. W. Voorhees, *Acta Mater.* **2014**, *70*, 66.
- [154] L. K. Aagesen, J. L. Fife, E. M. Lauridsen, P. W. Voorhees, *Scr. Mater.* **2011**, *64*, 394.
- [155] M. Yang, S. M. Xiong, Z. Guo, *Acta Mater.* **2015**, *92*, 8.
- [156] G. Requena, K. Bugelnig, F. Sket, S. Milenkovic, G. Rödler, A. Weisheit, J. Gussone, J. Haubrich, P. Barriobero-Vila, T. Pusztai, L. Gránásy, A. Theofilatos, J. C. da Silva, U. Hecht, *Addit. Manuf.* **2020**, *33*, 101133.
- [157] E. Y. Guo, A. B. Phillion, B. Cai, S. S. Shuai, D. Kazantsev, T. Jing, P. D. Lee, *Acta Mater.* **2017**, *123*, 373.
- [158] T. Subroto, C. L. Mendis, F. D'Elia, G. Szakács, J. L. Fife, N. Hort, K. U. Kainer, D. Tolnai, in *Magnesium Technology 2017* (Eds: K. N. Solanki, D. Orlov, A. Singh, N. R. Neelameggham), Springer International Publishing, Cham **2017**, p. 605.
- [159] M. A. Azeem, P. D. Lee, A. B. Phillion, S. Karagadde, P. Rockett, R. C. Atwood, L. Courtois, K. M. Rahman, D. Dye, *Acta Mater.* **2017**, *128*, 241.
- [160] M. Mukherjee, F. Garcia-Moreno, J. Banhart, *Scr. Mater.* **2010**, *63*, 235.
- [161] L. Arnberg, R. H. Mathiesen, *JOM* **2007**, *59*, 20.
- [162] R. H. Mathiesen, L. Arnberg, H. Nguyen-Thi, B. Billia, *JOM* **2012**, *64*, 76.
- [163] M. Ahmadein, M. Wu, G. Reinhart, H. Nguyen-Thi, A. Ludwig, presented at *4th Int. Conf. Advances in Solidification Processes (ICASP-4)*, Windsor UK **2016**.
- [164] Y. Chen, A.-A. Bogno, N. M. Xiao, B. Billia, X. H. Kang, H. Nguyen-Thi, X. H. Luo, D. Z. Li, *Acta Mater.* **2012**, *60*, 199.
- [165] S. McFadden, P. L. Schaffer, R. H. Mathiesen, D. J. Browne, *Mater. Sci. Forum* **2010**, *654–656*, 1359.
- [166] H. Nguyen-Thi, G. Reinhart, D. Browne, G. Zimmermann, R. Mathiesen, F. Kargl, W. H. Sillekens, in *In Situ X-ray Studies of Directional Solidification of Metal Alloys in Microgravity Conditions*, Visby, Schweden **2017**.
- [167] A. G. Murphy, R. H. Mathiesen, Y. Houtz, J. Li, C. Lockowandt, K. Henriksson, N. Melville, D. J. Browne, *J. Cryst. Growth* **2016**, *454*, 96.
- [168] M. Ahmadein, M. Wu, G. Reinhart, H. Nguyen-Thi, A. Ludwig, *IOP Conf. Ser.: Mater. Sci. Eng.* **2016**, *117*, 012010.
- [169] Y. Chen, A. A. Bogno, N. A. Xiao, B. Billia, X. H. Kang, H. Nguyen-Thi, X. H. Luo, D. Z. Li, *Acta Mater.* **2012**, *60*, 199.
- [170] A. J. Clarke, D. Tourret, Y. Song, S. D. Imhoff, P. J. Gibbs, J. W. Gibbs, K. Fezzaa, A. Karma, *Acta Mater.* **2017**, *129*, 203.
- [171] W. U. Mirihanage, K. V. Falch, I. Snigireva, A. Snigirev, Y. J. Li, L. Arnberg, R. H. Mathiesen, *Acta Mater.* **2014**, *81*, 241.
- [172] E. Maire, J. C. Grenier, D. Daniel, A. Baldacci, H. Klöcker, A. Bigot, *Scr. Mater.* **2006**, *55*, 123.
- [173] B. Cai, S. Karagadde, L. Yuan, T. J. Marrow, T. Connolley, P. D. Lee, *Acta Mater.* **2014**, *76*, 371.
- [174] C. Puncreobutr, P. D. Lee, K. M. Kareh, T. Connolley, J. L. Fife, A. B. Phillion, *Acta Mater.* **2014**, *68*, 42.
- [175] A. J. Shahani, X. Xiao, P. W. Voorhees, *Nat. Commun.* **2016**, *7*, 12953.
- [176] O. Ludwig, M. DiMichiel, L. Salvo, M. Suéry, P. Falus, *Metall. Mater. Trans. A* **2005**, *36A*, 1515.
- [177] B. Cai, J. Wang, A. Kao, K. Pericleous, A. B. Phillion, R. C. Atwood, P. D. Lee, *Acta Mater.* **2016**, *117*, 160.
- [178] C. Puncreobutr, A. B. Phillion, J. L. Fife, P. Rockett, A. P. Horsfield, P. D. Lee, *Acta Mater.* **2014**, *79*, 292.
- [179] J. W. Gibbs, K. A. Mohan, E. B. Gulsoy, A. J. Shahani, X. Xiao, C. A. Bouman, M. De Graef, P. W. Voorhees, *Sci. Rep.* **2015**, *5*, 11824.
- [180] R. Daudin, S. Terzi, P. Lhuissier, J. Tamayo, M. Scheel, N. H. Babu, D. G. Eskin, L. Salvo, *Acta Mater.* **2017**, *125*, 303.
- [181] R. Daudin, S. Terzi, P. Lhuissier, J. Tamayo, M. Scheel, N. Hari Babu, D. G. Eskin, L. Salvo, *Acta Mater.* **2017**, *125*, 303.
- [182] J. Campbell, *Castings: The New Metallurgy of Cast Metals*, Butterworth-Heinemann, Oxford, UK **2003**.
- [183] A. K. Gupta, B. K. Saxena, S. N. Tiwari, S. L. Malhotra, *J. Mater. Sci.* **1992**, *27*, 853.
- [184] N. Francois, Y. Zhang, R. Henley, L. Knuefing, R. Cruikshank, M. Turner, L. Beeching, A. Limaye, A. Kingston, M. Saadatfar, M. Knackstedt, *arXiv:2206.12763* **2022**.

- [185] J. Banhart, *Prog. Mater. Sci.* **2001**, *46*, 559.
- [186] J. Banhart, *Comprehensive Composite Materials II*, Elsevier, Oxford **2018**, p. 347.
- [187] F. García-Moreno, *Materials* **2016**, *9*, 85.
- [188] T.-H. Kang, K.-S. Kim, J.-Y. Yun, M.-J. Lee, K.-A. Lee, *Adv. Eng. Mater.* **2020**, *22*, 1901566.
- [189] M. F. Azamar, I. A. Figueroa, G. González, I. Alfonso, *J. Mater. Res.* **2021**, *37*, 225.
- [190] A. Sutygina, U. Betke, M. Scheffler, *Materials* **2019**, *12*, 3840.
- [191] A. Dudka, F. Garcia-Moreno, N. Wanderka, J. Banhart, *Acta Mater.* **2008**, *56*, 3990.
- [192] C. Körner, M. Arnold, R. F. Singer, *Mater. Sci. Eng., A* **2005**, *396*, 28.
- [193] K. Heim, G. S. Vinod-Kumar, F. García-Moreno, A. Rack, J. Banhart, *Acta Mater.* **2015**, *99*, 313.
- [194] K. Heim, F. García-Moreno, J. Banhart, *Scr. Mater.* **2018**, *153*, 54.
- [195] L. Helfen, T. Baumbach, H. Stanzick, J. Banhart, A. Elmoutaouakkil, P. Cloetens, *Adv. Eng. Mater.* **2002**, *4*, 808.
- [196] K. Mader, R. Mokso, C. Raufaste, B. Dollet, S. Santucci, J. Lambert, M. Stapanoni, *Colloids Surf., A* **2012**, *415*, 230.
- [197] L. Salvo, G. Martin, M. Suard, A. Marmottant, R. Dendievel, J.-J. Blandin, *C. R. Phys.* **2014**, *15*, 662.
- [198] A. H. Benouali, L. Froyen, T. Dillard, S. Forest, F. N'guyen, *J. Mater. Sci.* **2005**, *40*, 5801.
- [199] M. A. Islam, M. A. Kader, P. J. Hazell, A. D. Brown, M. Saadatfar, M. Z. Quadir, J. P. Escobedo, *Mater. Sci. Eng., A* **2016**, *666*, 245.
- [200] M. A. Islam, A. D. Brown, P. J. Hazell, M. A. Kader, J. P. Escobedo, M. Saadatfar, S. Xu, D. Ruan, M. Turner, *Int. J. Impact Eng.* **2018**, *114*, 111.
- [201] M. Kolluri, M. Mukherjee, F. Garcia-Moreno, J. Banhart, U. Ramamurty, *Acta Mater.* **2008**, *56*, 1114.
- [202] N. Wang, E. Maire, X. Chen, J. Adrien, Y. Li, Y. Amani, L. Hu, Y. Cheng, *Mater. Charact.* **2019**, *147*, 11.
- [203] N. Wang, X. Chen, E. Maire, P. H. Kamm, Y. Cheng, Y. Li, F. García-Moreno, *Adv. Eng. Mater.* **2020**, *22*, 2000264.
- [204] N. Wang, M. A. Noack, P. H. Kamm, J. Banhart, F. García-Moreno, *Adv. Eng. Mater.* **2022**, *24*, 2100795.
- [205] G. Costanza, F. Giudice, A. Sili, M. E. Tata, *Metals* **2021**, *11*, 1370.
- [206] T. R. Neu, P. H. Kamm, N. von der Eltz, H.-W. Seeliger, J. Banhart, F. García-Moreno, *Mater. Sci. Eng., A* **2021**, *800*, 140260.
- [207] T. Fiedler, E. Solorzano, F. Garcia-Moreno, A. Ochsner, I. V. Belova, G. E. Murch, *Adv. Eng. Mater.* **2009**, *11*, 843.
- [208] S. Xie, P. Xu, W. Cai, H.-E. Chen, H. Zhou, Z. Chen, T. Uchimoto, T. Takagi, *Int. J. Appl. Electromagn. Mech.* **2018**, *1*, 1.
- [209] M. Doroszko, A. Seweryn, *Mater. Sci. Eng., A* **2017**, *689*, 142.
- [210] J. Luksch, T. Bleistein, K. Koenig, J. Adrien, E. Maire, A. Jung, *Acta Mater.* **2021**, *208*, 116739.
- [211] G. S. Vinod Kumar, M. Mukherjee, F. Garcia-Moreno, J. Banhart, *Metall. Mater. Trans. A* **2013**, *44*, 419.
- [212] F. García-Moreno, J. Banhart, *Adv. Eng. Mater.* **2021**, *23*, 2100242.
- [213] M. Mukherjee, U. Ramamurty, F. Garcia-Moreno, J. Banhart, *Acta Mater.* **2010**, *58*, 5031.
- [214] M. Mukherjee, F. Garcia-Moreno, J. Banhart, *Metall. Mater. Trans. B* **2010**, *41*, 500.
- [215] C. Jiménez, F. Garcia-Moreno, M. Mukherjee, O. Goerke, J. Banhart, *Scr. Mater.* **2009**, *61*, 552.
- [216] C. Jiménez, M. Plaepow, P. H. Kamm, T. Neu, M. Klaus, G. Wagener, J. Banhart, C. Genzel, F. García-Moreno, *J. Synchrotron Radiat.* **2018**, *25*, 1790.
- [217] F. García-Moreno, M. Mukherjee, C. Jiménez, A. Rack, J. Banhart, *Metals-Basel* **2012**, *2*, 10.
- [218] F. Garcia-Moreno, E. Solorzano, J. Banhart, *Soft Matter* **2011**, *7*, 9216.
- [219] H. M. Helwig, F. Garcia-Moreno, J. Banhart, *J. Mater. Sci.* **2011**, *46*, 5227.
- [220] Z. Q. Guo, D. H. Ma, X. G. Yuan, X. Dong, *Rare Met. Mater. Eng.* **2016**, *45*, 3068.
- [221] A. V. Byakova, S. V. Gnyloskurenko, T. Nakamura, *Mater. Trans.* **2017**, *58*, 249.
- [222] X. Li, Y. Liu, J. Ye, X. An, Z. Cao, X. Liu, *Mater. Lett.* **2018**, *210*, 350.
- [223] F. García-Moreno, C. Jimenez, P. H. Kamm, M. Klaus, G. Wagener, J. Banhart, C. Genzel, *J. Synchrotron Radiat.* **2013**, *20*, 809.
- [224] P. H. Kamm, F. García-Moreno, T. R. Neu, K. Heim, R. Mokso, J. Banhart, *Adv. Eng. Mater.* **2017**, *19*, 1600550.
- [225] P. H. Kamm, T. R. Neu, F. García-Moreno, J. Banhart, *Acta Mater.* **2021**, *206*, 116583.
- [226] A. Myagotin, L. Helfen, T. Baumbach, *Meas. Sci. Technol.* **2009**, *20*, 055703.
- [227] E. Andrews, W. Sanders, L. J. Gibson, *Mater. Sci. Eng., A* **1999**, *270*, 113.
- [228] J. L. Grenestedt, *J. Mater. Sci.* **2005**, *40*, 5853.
- [229] U. Ramamurty, A. Paul, *Acta Mater.* **2004**, *52*, 869.
- [230] C. Leyens, J. Standfuß, A. Wetzig, F. Brückner, M. Barbosa, J. Hauptmann, E. Lopez, M. Seifert, D. Dittrich, P. Herwig, H. Hillig, L. Stepien, S. Gruber, *PhotonicsViews* **2021**, *18*, 32.
- [231] F. Fetzer, M. Sommer, R. Weber, J.-P. Weberpals, T. Graf, *Opt. Lasers Eng.* **2018**, *108*, 68.
- [232] D. Dittrich, A. Jahn, J. Standfuss, E. Beyer, *J. Laser Appl.* **2017**, *29*, 022425.
- [233] S. Börner, D. Dittrich, P. Mohlau, C. Leyens, F. García-Moreno, P. H. Kamm, T. R. Neu, C. M. Schlepuetz, *J. Laser Appl.* **2021**, *33*, 012026.
- [234] J. O. Milewski, *Additive Manufacturing of Metals*, Springer, New York **2017**.
- [235] C. Zhang, F. Chen, Z. Huang, M. Jia, G. Chen, Y. Ye, Y. Lin, W. Liu, B. Chen, Q. Shen, L. Zhang, E. J. Lavernia, *Mater. Sci. Eng., A* **2019**, *762*, 138209.
- [236] J. Plocher, A. Panesar, *Mater. Des.* **2019**, *183*, 108164.
- [237] P. Berger, H. Hülge, T. Graf, *Phys. Procedia* **2011**, *12*, 241.
- [238] J. L. Huang, N. Warnken, J.-C. Gebelin, M. Strangwood, R. C. Reed, *Acta Mater.* **2012**, *60*, 3215.
- [239] C. Zhao, N. D. Parab, X. Li, K. Fezzaa, W. Tan, A. D. Rollett, T. Sun, *Science* **2020**, *370*, 1080.
- [240] D. Wallerstein, A. Salminen, F. Lusquinos, R. Comesaña, J. D. V. García, A. R. Rodríguez, A. Badaoui, J. Pou, *Metals* **2021**, *11*, 622.
- [241] M. Gao, Y. Kawahito, S. Kajii, *Opt. Express* **2017**, *25*, 13539.
- [242] L. Aucott, D. Huang, H. B. Dong, S. W. Wen, J. A. Marsden, A. Rack, A. C. F. Cocks, *Sci. Rep.* **2017**, *7*, 40255.
- [243] C. Hagenlocher, J. Lind, R. Weber, T. Graf, *Appl. Sci.* **2020**, *10*, 2077.
- [244] M. Boley, F. Abt, R. Weber, T. Graf, *Phys. Procedia* **2014**, *41*, 488.
- [245] S. R. Stock, *Microcomputed Tomography: Methodology and Applications*, CRC Press, Boca Raton **2020**.
- [246] M. Benedetti, A. du Plessis, R. O. Ritchie, M. Dallago, S. M. J. Razavi, F. Berto, *Mater. Sci. Eng., R* **2021**, *144*, 100606.
- [247] A. du Plessis, S. M. J. Razavi, M. Benedetti, S. Murchio, M. Leary, M. Watson, D. Bhate, F. Berto, *Prog. Mater. Sci.* **2022**, *125*, 100918.
- [248] A. Thompson, I. Maskery, R. K. Leach, *Meas. Sci. Technol.* **2016**, *27*, 072001.
- [249] A. du Plessis, I. Yadroitsava, I. Yadroitsev, *Mater. Des.* **2020**, *187*, 108385.
- [250] G. Del Guercio, M. Galati, A. Saboori, P. Fino, L. Iuliano, *Acta Metall. Sinica* **2020**, *33*, 183.
- [251] Y. Amani, S. Dancette, P. Delroisse, A. Simar, E. Maire, *Acta Mater.* **2018**, *159*, 395.
- [252] M. Doroszko, *Materials* **2022**, *15*, 4807.
- [253] C. Kenel, T. Davenport, X. Li, R. N. Shah, D. C. Dunand, *Acta Mater.* **2020**, *193*, 51.

- [254] L. Zhao, S. Ha, K. W. Sharp, A. B. Geltmacher, R. W. Fonda, A. H. Kinsey, Y. Zhang, S. M. Ryan, D. Erdeniz, D. C. Dunand, K. J. Hemker, J. K. Guest, T. P. Weihs, *Acta Mater.* **2014**, *81*, 326.
- [255] L. Liu, P. Kamm, F. García-Moreno, J. Banhart, D. Pasini, *J. Mech. Phys. Solids* **2017**, *107*, 160.
- [256] T. Sun, W. Tan, L. Chen, A. Rollett, *MRS Bull.* **2020**, *45*, 927.
- [257] C. Zhao, K. Fezzaa, R. W. Cunningham, H. Wen, F. De Carlo, L. Chen, A. D. Rollett, T. Sun, *Sci. Rep.* **2017**, *7*, 3602.
- [258] C. L. A. Leung, S. Marussi, R. C. Atwood, M. Towrie, P. J. Withers, P. D. Lee, *Nat. Commun.* **2018**, *9*, 1355.
- [259] C. Kenel, D. Grolimund, X. Li, E. Panepucci, V. A. Samson, D. F. Sanchez, F. Marone, C. Leinenbach, *Sci. Rep.* **2017**, *7*, 16358.
- [260] N. D. Parab, C. Zhao, R. Cunningham, L. I. Escano, K. Fezzaa, W. Everhart, A. D. Rollett, L. Chen, T. Sun, *J. Synchrotron Rad.* **2018**, *25*, 1467.
- [261] Q. Guo, C. Zhao, M. Qu, L. Xiong, S. M. H. Hojjatzadeh, L. I. Escano, N. D. Parab, K. Fezzaa, T. Sun, L. Chen, *Addit. Manuf.* **2020**, *31*, 100939.
- [262] Y. Chen, S. J. Clark, C. L. A. Leung, L. Sinclair, S. Marussi, M. P. Olbinado, E. Boller, A. Rack, I. Todd, P. D. Lee, *Appl. Mater. Today* **2020**, *20*, 100650.
- [263] G. Additive, <https://www.ge.com/additive/blog/get-facts-porosity-metal-additive-manufacturing> (accessed: August 2022).
- [264] P. Lhuissier, X. Bataillon, C. Maestre, J. Sijbert, E. Cabrol, P. Bertrand, E. Boller, A. Rack, J.-J. Blandin, L. Salvo, G. Martin, *Addit. Manuf.* **2020**, *34*, 101271.
- [265] P. J. DePond, G. Guss, S. Ly, N. P. Calta, D. Deane, S. Khairallah, M. J. Matthews, *Mater. Des.* **2018**, *154*, 347.
- [266] S. A. Khairallah, A. T. Anderson, A. Rubenchik, W. E. King, *Acta Mater.* **2016**, *108*, 36.
- [267] V. Gunenthiram, P. Peyre, M. Schneider, M. Dal, F. Coste, I. Koutiri, R. Fabbro, *J. Mater. Process. Technol.* **2018**, *251*, 376.
- [268] M. Bayat, A. Thanki, S. Mohanty, A. Witvrouw, S. Yang, J. Thorborg, N. S. Tiedje, J. H. Hattel, *Addit. Manuf.* **2019**, *30*, 100835.
- [269] A. A. Martin, N. P. Calta, J. A. Hammons, S. A. Khairallah, M. H. Nielsen, R. M. Shuttlesworth, N. Sinclair, M. J. Matthews, J. R. Jeffries, T. M. Willey, J. R. I. Lee, *Mater. Today Adv.* **2019**, *1*, 100002.
- [270] A. A. Martin, N. P. Calta, S. A. Khairallah, J. Wang, P. J. Depond, A. Y. Fong, V. Thampy, G. M. Guss, A. M. Kiss, K. H. Stone, C. J. Tassone, J. Nelson Weker, M. F. Toney, T. van Buuren, M. J. Matthews, *Nat. Commun.* **2019**, *10*, 1987.
- [271] L. Sinclair, C. L. A. Leung, S. Marussi, S. J. Clark, Y. Chen, M. P. Olbinado, A. Rack, J. Gardy, G. J. Baxter, P. D. Lee, *Addit. Manuf.* **2020**, *36*, 101512.
- [272] M. Holler, M. Guizar-Sicairos, E. H. R. Tsai, R. Dinapoli, E. Müller, O. Bunk, J. Raabe, G. Aeppli, *Nature* **2017**, *543*, 402.
- [273] R. Bibb, J. Winder, *Radiography* **2010**, *16*, 78.
- [274] I. Campioni, I. Cacciotti, N. Gupta, *Annu. Ist. Super. Sanità.* **2020**, *56*, 10.
- [275] J. Wang, Y. Cui, C. Liu, Z. Li, Q. Wu, D. Fang, *J. Alloys Compd.* **2020**, *840*, 155753.
- [276] N. Asadizanjani, M. Tehranipoor, D. Forte, *IEEE Trans. Compon. Packag. Manuf. Technol.* **2017**, *7*, 292.
- [277] N. Nitta, F. Wu, J. T. Lee, G. Yushin, *Mater. Today* **2015**, *18*, 252.
- [278] M. Ebner, F. Marone, M. Stampanoni, V. Wood, *Science* **2013**, *342*, 716.
- [279] S.-M. Bak, Z. Shadike, R. Lin, X. Yu, X.-Q. Yang, *NPG Asia Mater.* **2018**, *10*, 563.
- [280] P. Pietsch, V. Wood, *Annu. Rev. Mater. Res.* **2017**, *47*, 451.
- [281] N. Seitzman, O. F. Bird, R. Andrykowski, S. Robbins, M. M. Al-Jassim, S. Pylypenko, *ACS Appl. Energy Mater.* **2021**, *4*, 1346.
- [282] J. Le Houx, D. Kramer, *Energy Rep.* **2021**, *7*, 9.
- [283] N. Shateri, D. J. Auger, A. Fotouhi, J. Brighton, W. Du, R. E. Owen, D. J. L. Brett, P. R. Shearing, *Batteries Supercaps* **2022**, *5*, e202200035.
- [284] J. Wang, C. Eng, Y.-C. K. Chen-Wiegart, J. Wang, *Nat. Commun.* **2015**, *6*, 7496.
- [285] V. Vanpeene, J. Villanova, A. King, B. Lestriez, E. Maire, L. Roué, *Adv. Mater.* **2019**, *9*, 1803947.
- [286] S. K. Wilke, D. C. Dunand, *J. Power Sources* **2020**, *448*, 227463.
- [287] K. E. Madsen, K. L. Bassett, K. Ta, B. A. Sforzo, K. E. Matusik, A. L. Kastengren, A. A. Gewirth, *Adv. Mater. Interfaces* **2020**, *7*, 2000751.
- [288] J. A. Lewis, F. J. Q. Cortes, Y. Liu, J. C. Miers, A. Verma, B. S. Vishnugopi, J. Tippens, D. Prakash, T. S. Marchese, S. Y. Han, C. Lee, P. P. Shetty, H.-W. Lee, P. Shevchenko, F. De Carlo, C. Saldana, P. P. Mukherjee, M. T. McDowell, *Nat. Mater.* **2021**, *20*, 503.
- [289] Y. Zhang, S. Chen, Y. Cai, L. Lu, D. Fan, J. Shi, J. Huang, S.-N. Luo, *Engineering* **2020**, *6*, 992.
- [290] P. R. Shearing, N. P. Brandon, J. Gelb, R. Bradley, P. J. Withers, A. J. Marquis, S. Cooper, S. J. Harris, *J. Electrochem. Soc.* **2012**, *159*, A1023.
- [291] F. Sun, K. Dong, M. Osenberg, A. Hilger, S. Risse, Y. Lu, P. H. Kamm, M. Klaus, H. Markötter, F. García-Moreno, T. Arlt, I. Manke, *J. Mater. Chem. A* **2018**, *6*, 22489.
- [292] G. A. Elia, G. Greco, P. H. Kamm, F. García-Moreno, S. Raoux, R. Hahn, *Adv. Funct. Mater.* **2020**, *30*, 2003913.
- [293] T. Yokoshima, D. Mukoyama, F. Maeda, T. Osaka, K. Takazawa, S. Egusa, *J. Electrochem. Soc.* **2019**, *166*, A1243.
- [294] D. Patel, J. B. Robinson, S. Ball, D. J. L. Brett, P. R. Shearing, *J. Electrochem. Soc.* **2020**, *167*, 090511.
- [295] L. Kong, X. Hu, G. Gui, Y. Su, M. Pecht, *Fire Technol.* **2020**, *56*, 2565.
- [296] D. P. Finegan, E. Darcy, M. Keyser, B. Tjaden, T. M. M. Heenan, R. Jervis, J. J. Bailey, N. T. Vo, O. V. Magdysyuk, M. Drakopoulos, M. Di Michiel, A. Rack, G. Hinds, D. J. L. Brett, P. R. Shearing, *Adv. Sci.* **2018**, *5*, 1700369.
- [297] D. P. Finegan, E. Darcy, M. Keyser, B. Tjaden, T. M. M. Heenan, R. Jervis, J. J. Bailey, R. Malik, N. T. Vo, O. V. Magdysyuk, R. Atwood, M. Drakopoulos, M. DiMichiel, A. Rack, G. Hinds, D. J. L. Brett, P. R. Shearing, *Energy Environ. Sci.* **2017**, *10*, 1377.
- [298] M. T. M. Pham, J. J. Darst, W. Q. Walker, T. M. M. Heenan, D. Patel, F. Iacoviello, A. Rack, M. P. Olbinado, G. Hinds, D. J. L. Brett, E. Darcy, D. P. Finegan, P. R. Shearing, *Cell Rep. Phys. Sci.* **2021**, *2*, 100360.
- [299] Y. Yang, Z. Xu, J. Steiner, Y. Liu, F. Lin, X. Xiao, *Appl. Phys. Lett.* **2020**, *116*, 081904.
- [300] D. P. Finegan, M. Scheel, J. B. Robinson, B. Tjaden, I. Hunt, T. J. Mason, J. Millichamp, M. Di Michiel, G. J. Offer, G. Hinds, D. J. L. Brett, P. R. Shearing, *Nat. Commun.* **2015**, *6*, 6924.
- [301] M. Eriksson, J. F. van der Veen, C. Quitmann, *J. Synchrotron Radiat.* **2014**, *21*, 837.
- [302] Excillum, <https://www.excillum.com/one-second-micro-ct/> (accessed: August 2022).
- [303] H. Xie, H. Luo, G. Du, C. Zhao, W. Xu, G. Zhou, R. Chen, T. Xiao, *J. Synchrotron Radiat.* **2019**, *26*, 1631.
- [304] Medipix, <https://medipix.web.cern.ch/home> (accessed: August 2022).
- [305] P. Villanueva-Perez, B. Pedrini, R. Mokso, P. Vagovic, V. A. Guzenko, S. J. Leake, P. R. Willmott, P. Oberta, C. David, H. N. Chapman, M. Stampanoni, *Optica* **2018**, *5*, 1521.
- [306] T. Shirasawa, L. Xiaoyu, W. Voegeli, E. Arakawa, K. Kajiwara, W. Yashiro, *Appl. Phys. Express* **2020**, *13*, 077002.
- [307] W. Yashiro, T. Shirasawa, C. Kamezawa, W. Voegeli, E. Arakawa, K. Kajiwara, *Jpn. J. Appl. Phys.* **2020**, *59*, 038003.
- [308] W. Voegeli, K. Kajiwara, H. Kudo, T. Shirasawa, X. Liang, W. Yashiro, *Optica* **2020**, *7*, 514.
- [309] D. M. Pelt, K. J. Batenburg, J. A. Sethian, *J. Imaging* **2018**, *4*, 128.

- [310] D. Wildenschild, A. P. Sheppard, *Adv. Water Res.* **2013**, *51*, 217.
- [311] H. Chan, M. Cherukara, T. Loeffler, B. Narayanan, S. Sankaranarayanan, *npj Comput. Mater.* **2020**, *6*, 1.
- [312] F. Marone, M. Stampanoni, *J. Synchrotron Rad.* **2012**, *19*, 1029.
- [313] K. A. Mohan, in *Development in X-Ray Tomography XI*, (Ed: B. Müller), Vol. 10391, SPIE Optical Engineering + Application Series **2017**, p. 103910U.
- [314] J.-W. Buurlage, F. Marone, D. M. Pelt, W. J. Palenstijn, M. Stampanoni, K. J. Batenburg, C. M. Schlepütz, *Sci. Rep.* **2019**, *9*, 18379.
- [315] V. Nikitin, A. Tekawade, A. Duchkov, P. Shevchenko, F. De Carlo, *J. Synchrotron Rad.* **2022**, *29*, 816.
- [316] T. Perciano, D. Ushizima, H. Krishnan, D. Parkinson, N. Larson, D. M. Pelt, W. Bethel, F. Zok, J. Sethian, *J. Synchrotron Rad.* **2017**, *24*, 1065.
- [317] D. Parkinson, D. Pelt, T. Perciano, D. Ushizima, H. Krishnan, H. Barnard, A. MacDowell, J. Sethian, in *Development in X-Ray Tomography XI*, (Ed: B. Müller), Vol. 10391, SPIE Optical Engineering + Application Series **2017**, p. 103910J.
- [318] M. Kobayashi, H. Toda, Y. Kawai, T. Ohgaki, K. Uesugi, D. S. Wilkinson, T. Kobayashi, Y. Aoki, M. Nakazawa, *Acta Mater.* **2008**, *56*, 2167.
- [319] S. Roux, F. Hild, P. Viot, D. Bernard, *Composites, Part A* **2008**, *39*, 1253.
- [320] A. Buljac, C. Jailin, A. Mendoza, J. Negggers, T. Taillandier-Thomas, A. Bouterf, B. Smaniotta, F. Hild, S. Roux, *Exp. Mech.* **2018**, *58*, 661.
- [321] E. Plancher, P. Gravier, E. Chauvet, J.-J. Blandin, E. Boller, G. Martin, L. Salvo, P. Lhuissier, *Acta Mater.* **2019**, *181*, 1.
- [322] H. Toda, E. Maire, Y. Aoki, M. Kobayashi, *J. Strain Anal. Eng. Des.* **2011**, *46*, 549.
- [323] T. Strohmann, K. Bugelnig, E. Breitbarth, F. Wilde, T. Steffens, H. Germann, G. Requena, *Sci. Rep.* **2019**, *9*, 19611.
- [324] A. A. Hendriksen, D. M. Pelt, W. J. Palenstijn, S. B. Coban, K. J. Batenburg, *Appl. Sci.* **2019**, *9*, 2445.



Francisco García-Moreno is a senior scientist and deputy head of the Institute of Applied Materials at the Helmholtz-Zentrum Berlin für Materialien und Energie. He holds a diploma and PhD in physics from the University of Göttingen and is a lecturer at the Technische Universität Berlin, where he leads a materials science research group. He developed a simultaneous, time-resolved X-ray imaging and diffraction method and is expert in X-ray tomography (time-resolved tomography). His research interests are focused on cellular and porous materials, complex fluids, solidification processes, alloy development, additive manufacturing and energy materials among others.



Tillmann Robert Neu is a postdoctoral researcher at the Institute of Material Sciences and Technology at the Technische Universität Berlin. He holds a B.Sc., M.Sc. and Dr.-Ing. in materials science from the Technische Universität Berlin. His research interests include cellular, porous and granular materials, solidification processes, additive manufacturing and alloy development. To study dynamic processes in-situ, he uses the technique of time-resolved tomography (tomoscopy), further advancing the temporal resolution.



Paul Hans Kamm is a postdoctoral researcher at the Institute of Applied Materials at the Helmholtz-Zentrum Berlin für Materialien und Energie. He holds a B.Sc., M.Sc. and Dr.-Ing. in materials science from the Technische Universität Berlin. His research interests include cellular, porous and granular materials, complex fluids, solidification processes and energy materials. To study dynamic processes in-situ, he uses the technique of time-resolved tomography (tomoscopy), further advancing the temporal resolution. As a beamline scientist at the Energy Dispersive Diffraction (EDDI) beamline at BESSY II, Berlin he co-developed the option for time-resolved and simultaneous imaging and diffraction.



John Banhart is the head of the Institute of Applied Materials at the Helmholtz-Zentrum Berlin für Materialien und Energie and of the Chair of Structure and Properties of Materials at the Technische Universität Berlin. Most of his work is focussed on light metallic materials and materials for energy conversion and storage as well as on methods needed to explore their structure. Among the materials studied are aluminum alloys and aluminum foams. The methods applied include imaging techniques such as radiography and tomography based on X-rays from tubes and synchrotron sources and neutrons.